REPORT DOCUMENTATION PAGE	Form Approved OMB NO. 0704-0188

The public reporting burden for this collection of information is estimated to average 1 hour per response, including the time for reviewing instructions, searching existing data sources, gathering and maintaining the data needed, and completing and reviewing the collection of information. Send comments regarding this burden estimate or any other aspect of this collection of information, including suggesstions for reducing this burden, to Washington Headquarters Services, Directorate for Information Operations and Reports, 1215 Jefferson Davis Highway, Suite 1204, Arlington VA, 22202-4302. Respondents should be aware that notwithstanding any other provision of law, no person shall be subject to any oenalty for failing to comply with a collection of information if it does not display a currently valid OMB control number.
PLEASE DO NOT RETURN YOUR FORM TO THE ABOVE ADDRESS.

1. REPORT DATE (DD-MM-YYYY) 08-10-2010	2. REPORT TYPE Final Report	3. DATES COVERED (From - To) 1-Jul-2008 - 30-Jun-2010

4. TITLE AND SUBTITLE	5a. CONTRACT NUMBER
Condensed Phase Product Penetration and Flame Spreading Processes in Granular Propellant Bed	W911NF-08-1-0176
	5b. GRANT NUMBER
	5c. PROGRAM ELEMENT NUMBER 611102

6. AUTHORS	5d. PROJECT NUMBER
Kenneth K. Kuo, Alexander Colletti, Matthew Sirignano, and Eric Boyer	
	5e. TASK NUMBER
	5f. WORK UNIT NUMBER

7. PERFORMING ORGANIZATION NAMES AND ADDRESSES	8. PERFORMING ORGANIZATION REPORT NUMBER
Pennsylvania State University Office of Sponsored Programs The Pennsylvania State University University Park, PA 16802 -7000	

9. SPONSORING/MONITORING AGENCY NAME(S) AND ADDRESS(ES)	10. SPONSOR/MONITOR'S ACRONYM(S) ARO
U.S. Army Research Office P.O. Box 12211 Research Triangle Park, NC 27709-2211	11. SPONSOR/MONITOR'S REPORT NUMBER(S) 53402-EG.1

12. DISTRIBUTION AVAILIBILITY STATEMENT

Approved for Public Release; Distribution Unlimited

13. SUPPLEMENTARY NOTES

The views, opinions and/or findings contained in this report are those of the author(s) and should not contrued as an official Department of the Army position, policy or decision, unless so designated by other documentation.

14. ABSTRACT

Understanding the detailed ignition, flame-spreading, and combustion processes inside of a granular solid-propellant bed is vital for accurate interior ballistic modeling, and for the development of ballistic propulsion systems. Experiments were conducted to investigate both the penetration characteristics of pyrotechnic igniter jets, and the subsequent flame spreading processes in a granular bed. The experiments utilized both live and inert propellant, in conjunction with high-speed photography and photodetectors. A singular igniter jet was discharged

15. SUBJECT TERMS

granular propellant bed, condensed-phase product depostion, black powder, flame spreading, ignition

16. SECURITY CLASSIFICATION OF:			17. LIMITATION OF ABSTRACT	15. NUMBER OF PAGES	19a. NAME OF RESPONSIBLE PERSON Kenneth Kuo
a. REPORT UU	b. ABSTRACT UU	c. THIS PAGE UU	UU		19b. TELEPHONE NUMBER 814-863-6270

Standard Form 298 (Rev 8/98)
Prescribed by ANSI Std. Z39.18

Report Title

Condensed Phase Product Penetration and Flame Spreading Processes in Granular Propellant Bed

ABSTRACT

Understanding the detailed ignition, flame-spreading, and combustion processes inside of a granular solid-propellant bed is vital for accurate interior ballistic modeling, and for the development of ballistic propulsion systems. Experiments were conducted to investigate both the penetration characteristics of pyrotechnic igniter jets, and the subsequent flame spreading processes in a granular bed. The experiments utilized both live and inert propellant, in conjunction with high-speed photography and photodetectors. A singular igniter jet was discharged axially into an inert granular bed. This setup was designed to study the region of particles coated by the condensed-phase products of the igniter jet. This information is very useful since the ignition behavior of live propellants is dependent upon both convective heating by the igniter jet as well as conductive heating by the deposited condensed-phase products. Three correlations were developed that describe the region of the granular bed coated by the condensed-phase products from the igniter jet; these include: 1) the axial depth of penetration, 2) maximum radial penetration, and 3) the volume of the coated region. These parameters were found as functions of the Reynolds number based on the operating conditions of the igniter jet and granular bed.

List of papers submitted or published that acknowledge ARO support during this reporting period. List the papers, including journal references, in the following categories:

(a) Papers published in peer-reviewed journals (N/A for none)

Number of Papers published in peer-reviewed journals: 0.00

(b) Papers published in non-peer-reviewed journals or in conference proceedings (N/A for none)

Number of Papers published in non peer-reviewed journals: 0.00

(c) Presentations

A. Colletti, E. Boyer, K.K. Kuo, and R. Acharya, "Design of a Modular Test Chamber for the Analysis of Flame Spreading Rates, Black Powder Jet Penetration, and Vent-Hole Geometry into a Granular Bed," presented at Eighth International Symposium on Special Topics in Chemical Propulsion (8-ISICP), Cape Town, South Africa, November 2-6, 2009.

Number of Presentations: 1.00

Non Peer-Reviewed Conference Proceeding publications (other than abstracts):

Number of Non Peer-Reviewed Conference Proceeding publications (other than abstracts):   0

Peer-Reviewed Conference Proceeding publications (other than abstracts):

Number of Peer-Reviewed Conference Proceeding publications (other than abstracts):   0

(d) Manuscripts

Alexander E. Colletti, Eric Boyer, Kenneth K. Kuo, and Matthew D. Sirignano, "Characterization of Black Powder Igniter Jets into a Granular Bed through Analysis of Condensed-Phase Product Deposition and Regions of Penetration," submitted to the International Journal of Energetic Materials and Chemical Propulsion, under review.

Number of Manuscripts: 1.00

Patents Submitted

Patents Awarded

Graduate Students

NAME	PERCENT SUPPORTED	
Alexander Colletti	1.00	
Matthew Sirignano	0.25	
FTE Equivalent:	**1.25**	
Total Number:	**2**	

Names of Post Doctorates

NAME	PERCENT_SUPPORTED	
Ragini Acharya	0.10	
FTE Equivalent:	**0.10**	
Total Number:	**1**	

Names of Faculty Supported

NAME	PERCENT_SUPPORTED	National Academy Member
Eric Boyer	0.25	No
Kenneth Kuo	0.04	No
FTE Equivalent:	**0.29**	
Total Number:	**2**	

Names of Under Graduate students supported

NAME	PERCENT_SUPPORTED	
Jeffrey Krug	0.05	
FTE Equivalent:	**0.05**	
Total Number:	**1**	

Student Metrics
This section only applies to graduating undergraduates supported by this agreement in this reporting period

The number of undergraduates funded by this agreement who graduated during this period: 1.00

The number of undergraduates funded by this agreement who graduated during this period with a degree in science, mathematics, engineering, or technology fields:...... 1.00

The number of undergraduates funded by your agreement who graduated during this period and will continue to pursue a graduate or Ph.D. degree in science, mathematics, engineering, or technology fields:...... 0.00

Number of graduating undergraduates who achieved a 3.5 GPA to 4.0 (4.0 max scale):...... 1.00

Number of graduating undergraduates funded by a DoD funded Center of Excellence grant for Education, Research and Engineering:...... 0.00

The number of undergraduates funded by your agreement who graduated during this period and intend to work for the Department of Defense 1.00

The number of undergraduates funded by your agreement who graduated during this period and will receive scholarships or fellowships for further studies in science, mathematics, engineering or technology fields:...... 0.00

Names of Personnel receiving masters degrees

NAME

Alexander Colletti

Total Number: **1**

Names of personnel receiving PHDs

NAME

Total Number:

Names of other research staff

NAME	PERCENT_SUPPORTED	
Scott Blakeslee	0.05	No
Baoqi Zhang	0.12	No
FTE Equivalent:	**0.17**	
Total Number:	**2**	

Sub Contractors (DD882)

Inventions (DD882)

Table of Contents:

Appendices:

Figures:

Tables:

Equations:

1. Nomenclature

d_{jet}	Jet-orifice diameter
d_{part}	Particle diameter
L	Depth of penetration of condensed phase
$\bar{P}$	Average pressure from initial rise to blowdown cut-off level
P_{atm}	Back pressure of atmospheric as initial pressure
$Re_{d_{jet}}$	Reynolds number based on the jet-orifice diameter
U_{jet}	Gas velocity at jet orifice
$V_{covered}$	The volume of the region coated by condensed-phase products
V_{part}	The volume of a single inert spherical particle

Greek

μ_{jet}	Viscosity of the gas jet
ρ_{jet}	Density of the igniter jet at the jet orifice

2. Introduction

In various ballistic propulsion systems, a pyrotechnic igniter (commonly containing black-powder pellets) is usually employed to achieve the ignition of granular solid propellants loaded in a cartridge. The use of granular solid propellant beds in these applications in lieu of solid propellant grains is due to their ability to pressurize the combustion chamber more rapidly. For ballistic application, high rates of pressurization are often desired.

Combustion of solid propellants in a granular bed with high specific burning surface area can achieve rapid pressurization rates compared to bulk solid propellant grains. In a packed bed, the combustion of the propellant grains is further augmented by convective heat transfer process, which is enabled by the penetrating gas and hot particles flowing through the interstitial spacing between granular particles. The process of convective burning is "a deflagration wave whose propagation rate is control by convective heat transfer via rapid, deep penetration of hot gases, instead of diffusional processes only (Asay et al., 2001)." As a result the combustion of a granular bed can be expected to occur several orders of magnitude more quickly than a rocket motor.

Inside of a granular solid-propellant bed, the detailed processes of ignition, flame spreading, and combustion are very complex. Part of this complexity is caused by the nature of black-powder products, which contain both gas and condensed phases. Typically the gas-phase products of black powder contain CO_2, N_2, CO, H_2O, KOH, SO_2, S_2, etc. The condensed-phase products of black powder contain $K_2S_{(l)}$, $K_2CO_{3(l)}$, $K_2SO_{4(l)}$, $CaO_{(s)}$, etc. In order to achieve ignition in a cartridge, the granular propellants loaded in the neighborhood of the vent holes of the igniter system are heated intensely by discharging jets of the aforementioned black-powder combustion products. The detailed interactions of a discharging jet with the adjacent granular propellant particles are not well characterized, as it is generally difficult to have optical access to their interfacial locations. The gas-phase products can easily penetrate the granular bed through interstitial voids, and heat the granular propellants by the convective heat-transfer mechanism. However, the condensed-phase products from the black powder can deposit directly onto the surfaces of the neighboring granular propellants, thus producing a coated layer of hot liquid that provides direct conductive heat transfer to the unburned granular propellants. Prior to this study, the extent of the region coated by the jet was unknown.

In addition to the gap in knowledge regarding the specifics of the igniter jet penetration process, the flame spreading that occurs from the ignited zone to the unburnt propellants is also not well characterized. The flame spreading processes are not easily visible due to the presence of high-temperature and high-pressure gases generated from the combustion process.

The goal of this project was to acquire this important information, which is beneficial to the modeling and simulation of the complex ignition process found in granular solid-propellant beds. Higher fidelity modeling allows for achieving more realistic simulations, and cost effective design processes. The use of these achievements, coupled with a deeper understanding of interior ballistic processes will ultimately allow for the development of ballistic propulsion systems that are more reliable, accurate, and safe to operate.

Although there have been recent studies on loading density (i.e. the volume of propellant to chamber volume) (Williams et al, 2006) and one-dimensional flame spreading (Kooker et al, 1993), there has been little experimental work on flame propagation in three dimensions or the

2

enhancement of heat transfer rates to the ball propellant from the condensed phase products in the black powder igniter jet. This information is especially pertinent because recent numerical models (Acharya and Kuo, 2007) have been required to use one-dimensional approximations for jet penetration or assumptions for the two-phase flow heat transfer characteristics (Porterie and Loraud, 1994). Particularly, the degree and phase of the black-powder product jet penetration into the granular bed, flame spreading rates, and the effects of vent-hole geometry on those factors have not been well developed.

The objectives of the experiments designed and conducted for this investigation were to:

   1) Observe the igniter jet penetration into the granular bed

   2) Characterize the penetration process of the condensed-phase products into the granular bed through correlation of the geometric parameters of the region coated by the condensed-phase product species with the operating conditions of the igniter jet.

   3) Observe and measure the flame spreading rates in the radial, azimuthal, and axial directions.

Ultimately, the goal is to enhance the understanding of the interior ballistic phenomena of the gaseous and condensed-phase products into the granular bed. The experimental data and observational results can be utilized to provide useful information for detailed numerical simulation.

3. Modular Test Rig
To observe and characterize the relevant interior ballistics phenomena involved in the ignition and subsequent combustion of a granular solid-propellant bed, a test rig was designed, fabricated, and utilized. The experimental test rig was designed so that it could operate on the test stand already available at the High Pressure Combustion Lab (HPCL) where previous mortar experiments have been performed (Figure 1). The key features incorporated are:

- Reusable test chamber;
- Pressure taps for the igniter and granular bed sections;
- Modular granular bed test sections to allow for investigation of axial, radial, or azimuthal flame spreading;
- Windowed access to the burning granular propellant bed which is transparent to both the visible and near-IR radiation.
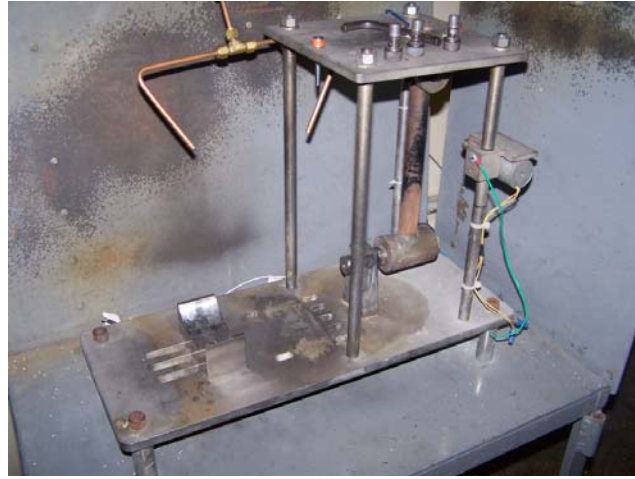
Figure 1: HPCL test stand for various mortar tests.

3.1 Head End and Ignition Train

Common to all tests performed is the head end of the test section shown in Figure 2. The ignition system is located in this section of the test rig, which houses a firing pin, a brass cartridge holding a percussion primer, and a pyrotechnic igniter chamber for loading a desired number of center-perforated black-powder pellets.
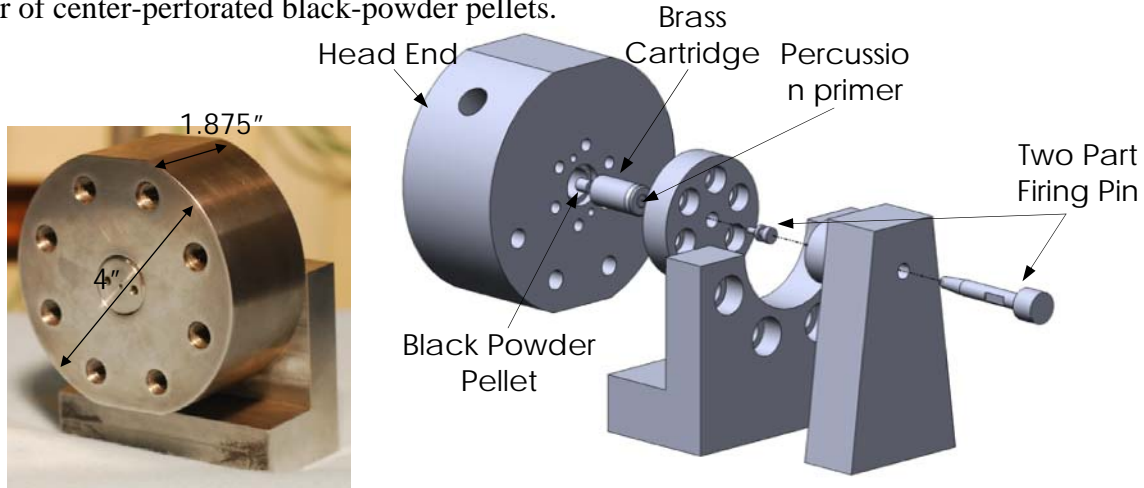
Figure 2: (Left) Head end of test rig with L-shaped bracket and the interchangeable flash-tube vent section installed. (Right) Exploded view of head end section showing the two part firing pin.

Operation of the system starts with the impact of a swinging pendulum (seen on the right in Figure 1) that strikes the firing pin into the base of the percussion primer. The combustion products generated from the primer ignite the black-powder pellets in the flash tube. The discharge of the combustion products from the primer and black-powder pellets is controlled by one of several interchangeable components, depicted in Figure 3, which contain either one or multiple vent holes in different configurations (e.g., a singular axial vent hole, or two radial vent

holes). This discharge was instrumented by a dynamic piezoelectric pressure transducer located in the flash tube section and it was used to characterize the strength of the jet.
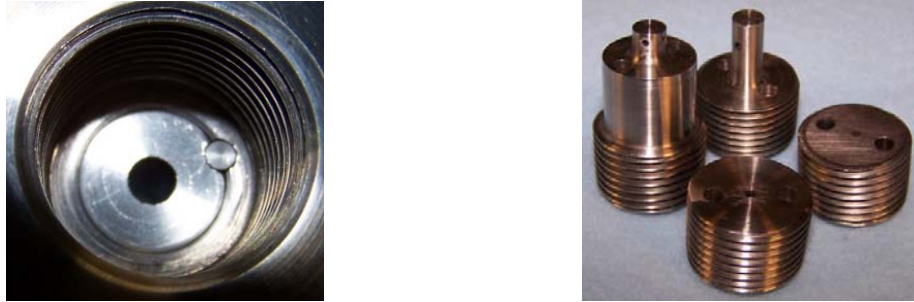
Figure 3: (Left) Threading for installation of interchangeable flash-tube vent section (installed flash tube section with steel alignment pin also shown). (Right) Interchangeable flash-tube vent sections with various orifice configurations.

The percussion primer is the Fedral No. 150 large pistol primer. This primer is most notably used in .45 ACP pistol cartridges, but also begins the ignition train in the 120 mm mortar system. The brass gun cartridge is designed to expand and seal hot gases while also being reusable. Therefore, this component is used directly to hold the primer in the head end. The cartridge sits over the black powder retainer which holds up to one black-powder pellet. This simple part is modular and can be replaced to allow for different geometries or quantities of pellets to be used. Based upon the experience of HPCL members with Army's 120 mm mortar, the pressure developed from these components was expected to be 20 to 28 MPa. However, due to backflow from the main section of the chamber, this section needed to be able to withstand the maximum chamber pressure. It was therefore designed for a maximum static pressure of 138 MPa with a minimum factor of safety of 4. With this strength consideration, there was a need for hard steel which could resist deformation to seal the cartridge, and for corrosion resistance, a 17-4 PH stainless steel was chosen.

3.2 Radial/Azimuthal Test Configuration

The radial configuration for the test rig was the first configuration created and was designed to investigate radial and azimuthal flame spreading. A cross-sectional view and an exploded view of the test rig are shown in Figure 4. The main chamber is created from the same 17-4 PH stainless steel as the head end to support the 103 MPa of pressure expected from the combustion of the granular bed (again the pressure was based on previous experience from PSU mortar tests). The chamber is axisymmetric with four exit ports and four pressure taps distributed uniformly along the outer circumference of the chamber.
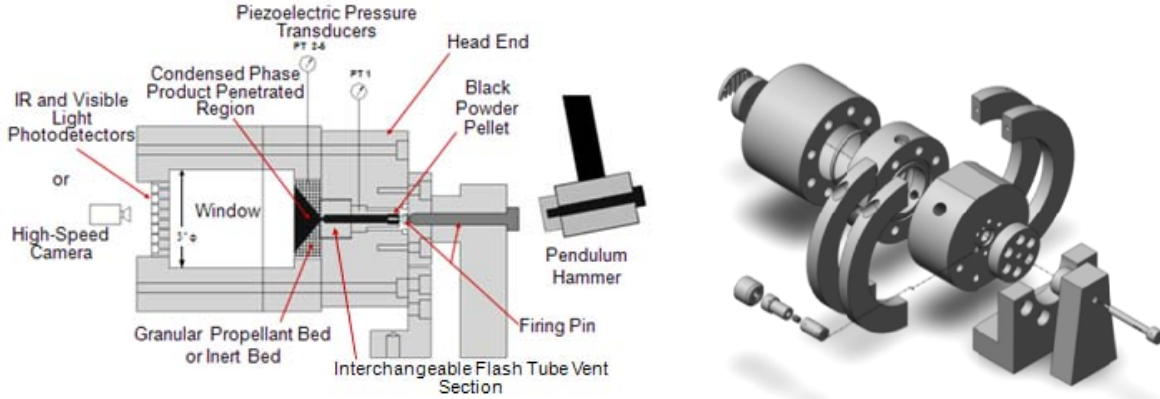
Figure 4: Cross-sectional and exploded views of the modular flame-spreading test rig in its radial/azimuthal configuration with a central axial vent hole on the interchangeable flash-tube vent section.

When assembled, the main chamber section and window support hold three windows in place. The first is a sacrificial window made of borosilicate glass. This member is not expected to hold the chamber pressure and is typically destroyed by the intense pressure and temperature of each test. The next two members are quartz; they are designed to hold the full chamber pressure and are reusable after each test. Both types of windows are transparent to the spectral emissions of interest.

An array of photodetectors or a high-speed camera sits directed at the windows in this configuration (shown in Figure 4). The spacing of the sensor ports for the photodetectors was developed to allow a maximum amount of the physically larger IR photodetectors to view the event. A plastic spacer sits in this port to allow the visible light photodiode to be seated in the same position. The diagram of the photodetector array is shown in Figure 5.
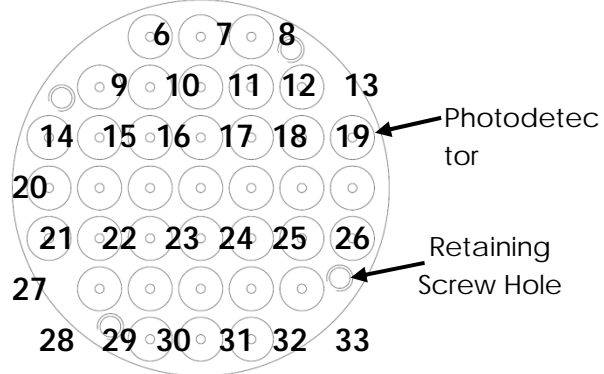
Figure 5: End view of an array of photodetectors with positional numbering (positions 1-5 were used for pressure transducer locations and therefore not shown in this diagram).

3.3 Condensed-Phase Deposition Configuration

This configuration of the modular test rig was a modification of the radial configuration and was used for experiments that focused on the characterization of the region of deposition by the condensed-phase products of the igniter jet. A cross-sectional view is shown in Figure 6.

The main test chamber section from the radial/azimuthal configuration was removed and the window support section was utilized to contain an inert granular bed instead of to hold the window assembly. A semi-permeable covering (in this case stiff paper) was placed over the viewing port to hold the inert bed in place but allow hot gases to exit. This was an ideal configuration because the gas path that must be taken to leave the chamber was downstream of the area of interest and did not affect the fluid dynamics governing the condensed-phase deposition.

A	Firing pin
B	Test mounting stand
C	Head end
D	Percussion primer
E	Black powder pellet
F	Flash Tube
G	Orifice
H	Granular propellant bed
I	Cardboard barrier
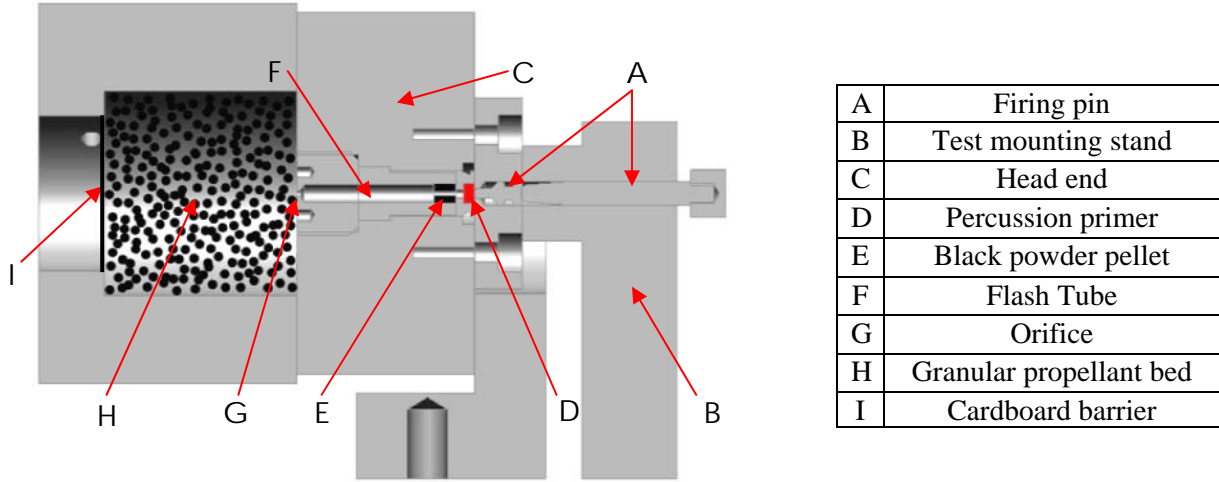
Figure 6: Cross-sectional view of the modular test rig in the configuration used to study condensed-phase product deposition from an igniter jet.

3.4 Axial Configuration

The axial configuration also attaches to the head end. A cross-sectional and an exploded view are shown in Figures 7 and 8 respectively. It is designed to allow flame spreading for 11.621 cm in a 1.778 cm diameter cylinder. The propellant is sealed into place inside of the cylinder by a steel burst disk held in place by a vented bolt. When the chamber reaches a specified pressure, the burst disk will fail, in shear, allowing hot gases and particles to rapidly escape. Different pressures can be reached by varying the thickness of the burst disks or amount of propellant in the chamber.
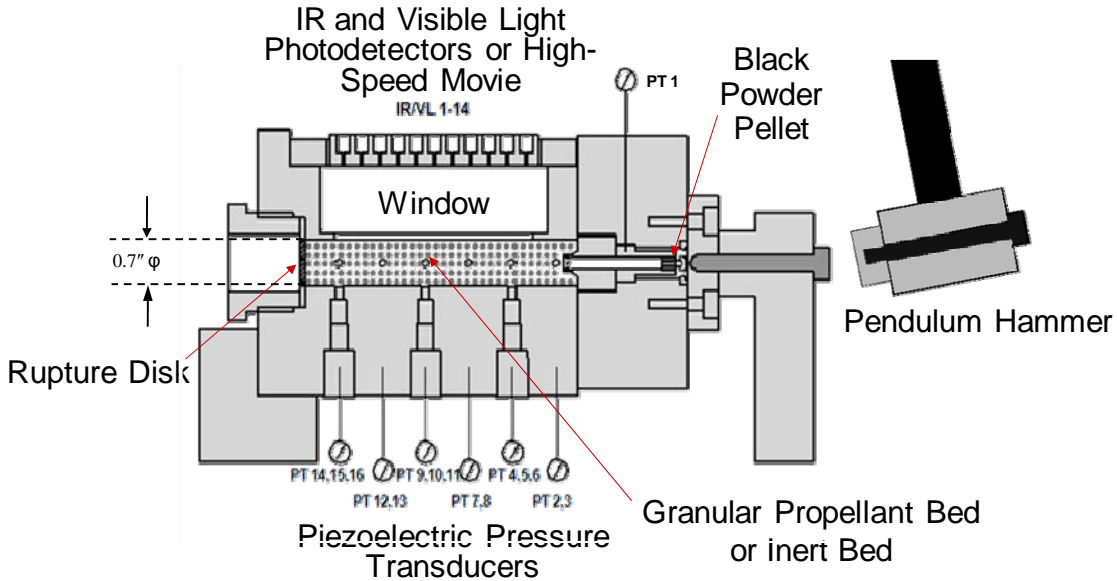
Figure 7: Cross-sectional view of the modular test rig in the configuration used to study axial flame spreading.
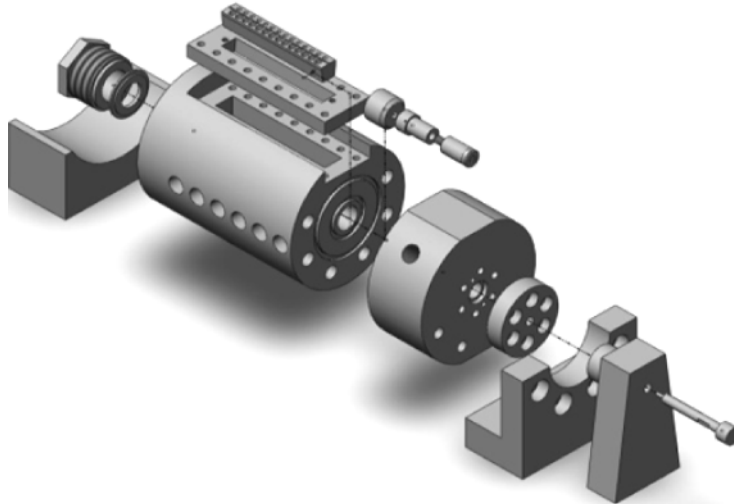
Figure 8: Exploded view of the modular test rig in the configuration used to study axial flame spreading.

In order to observe the flame-spreading event, there is an 8.458 cm long window cutout along the axis of the cylinder. Similar to the radial/azimuthal setup, there is a borosilicate sacrificial window followed by two quartz windows. Above these windows sits the detector array. It is designed with a number of axial positions, and each axial position can be monitored by both a visible light photodiode and an infrared light photodetector simultaneously. This is accomplished by setting the detectors and their apertures at an angle. In addition to the photodetector array 15 pressure taps were arranged both axially down the chamber and at various locations about its circumference to facilitate the measurement of the chamber pressure from a variety of locations.

8

4. Method of Approach

4.1 Diagnostics

All tests were instrumented with a minimum of both piezoelectric pressure transducers and a trigger signal from the test. The signals were measured on one of two data acquisition systems (DAQ), either a Nicolet Vision or a Nicolet MultiPro. The pressure transducers used were PCB 111A23s capable of sampling pressures of up to 138 MPa at a rate of 100 kHz.

To create a common initial time among different tests, a 5-Volt trigger signal was generated when the pendulum hammer head struck the firing pin. This reference signal was created by an ultra-low-current digital continuity circuit and allowed the measurement and comparison of ignition delays and flame-spreading events. The circuit uses a NAND (negated AND) gate to transform the voltage change caused by the hammer striking the firing pin and completing a circuit to ground to a digital signal. However, mechanical friction in the system (between the hammer strike, the first firing pin, and the secondary pin striking the primer) keeps the repeatability from being as low as possible. The mechanical delay may change the time of the trigger signal by up to 0.5 ms. It was therefore mainly used as a common signal when it was necessary to simultaneously operate a combination of multiple data acquisition systems, including the high-speed camera.

To measure the signal from both the visible light photodiodes (Perkin-Elmer VTP3310LA) and the infrared light photodetectors (EOS PBSE-010) a voltage divider circuit was created. The signal was measured though a unity-gain op-amp buffer to prevent the high-impedance data acquisition system from influencing the measurement circuit. An adjustable voltage divider was also created so that the signal could be read differentially, thus nearer to the center of the DAQ's range. This allowed a smaller voltage range, and thus, higher resolution measurements to be taken.

As an alternative to the photodetectors, a high-speed digital camera is also used to view the flame-spreading event. It is a Photron FastCam PCI and can capture images at up to 2000 frames per second. This gives higher spatial resolution than the photodetectors but lower resolution in time.

To minimize signal distortion from the flame-spreading event to the optical diagnostics, the window interfaces are filled with low viscosity mineral oil for every test. This has an index of refraction close to that of the quartz windows (near 1.45) and provides for a much better interface than air (index of refraction close to 1).

4.2 Igniter Characterization

In order to establish a baseline for the behavior of the igniter jet without the presence of a propellant bed, the head end was tested independently with an axial interchangeable flash-tube section. The head end was tested with two different propellant configurations. The first was with only the pistol primer, the second included a black-powder pellet. The head end section was instrumented only with the pressure transducer located in the flash tube section. The event was also captured using high-speed photography.

4.3 Azimuthal Flame Spreading

To conduct the azimuthal flame-spreading experiments, the radial/azimuthal configuration of the modular test rig was utilized. The interchangeable flash-tube vent section that was used contained two radially oriented jet orifices, each with a diameter of 1.65mm. The orifices were diametrically opposite to create a symmetric area of igniter-jet penetration. The flash-tube vent section extended into the granular bed to initiate combustion directly in front of the sacrificial window. A picture of the used interchangeable flash-tube vent section is shown in Figure 9.

Radial Vent Hole →
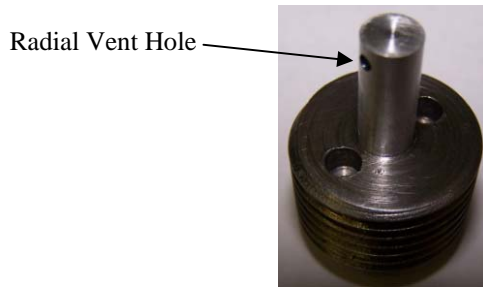
Figure 9: The interchangeable flash-tube vent section with a dual radial jet configuration used in the azimuthal flame spreading experiments.

Tests were conducted with two configurations of the propellant bed: 1) completely inert granular propellants, and 2) with only two layers of live propellant grains adjacent to the sacrificial window and the remainder of the bed was filled by inert particles. The first configuration was used to observe the penetration of the igniter jets through the granular bed. As the igniter jets did not react with the granular bed in this configuration, only the luminous products from the igniter jet are observable during the test. The reason for using such limited quantities of live propellant, in the second configuration, was to avoid over pressurization while still being able to observe the initial jet penetration and flame spreading event. In order to capture the initial jet penetration event, either the array of photodetectors (visible light or infrared) or the high-speed camera was used. The radial/azimuthal test rig is shown mounted on the test stand in Figure 10.
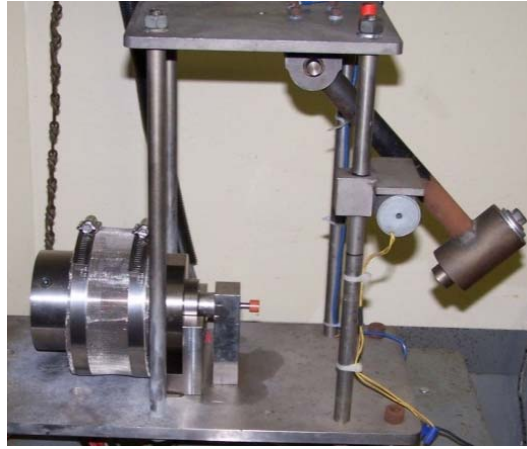
Figure 10: Radial/Azimuthal test rig configuration installed on test stand at HPCL.

4.4 Axial Flame Spreading

The utilized interchangeable flash-tube section was designed to turn the flow 90° through four axi-symmetric vent holes (diameter = 1.02 mm), shown in Figure 11. This creates a planar gas-phase ignition wave in the granular bed so that pure axial flame spreading can be examined. It extends past the face of the head end section of the test rig with a solid cylinder to fill some of the axial chamber. This allows the granular bed, and igniter jets, to begin directly below the window port.

Radial Vent Hole

Radial Vent Hole

Figure 11: Flash-tube vent section with four axi-symmetric, radial vent holes used for the axial flame-spreading experiments.

Similarly to the azimuthal flame-spreading experiments, the chamber was only partially filled with live propellant while the remainder was filled with an inert propellant simulant. The amount of live propellant varied from 2.5 to 4.5 grams, and the ignition train contained either one or one half of a black-powder pellet. Five pressure transducers were installed in the axial chamber's pressure taps. The most common reference locations used were PT 2, 4, 7, 9, 12, and 14. These locations correspond to an axial distance of 0.93, 2.78, 4.63, 6.48, 8.33, and 10.19 cm downstream of the face of the head end section.   The axial test rig is shown mounted on the test stand in Figure 12.
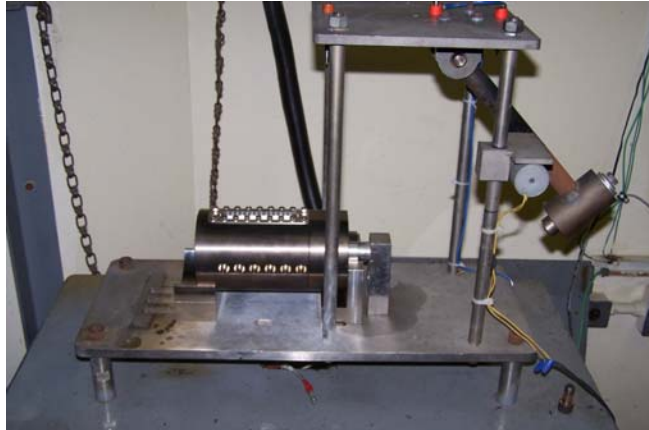
Figure 12: Axial test rig configuration installed on test stand at HPCL.

4.5 Characterization of Condensed-Phase Deposition

As mentioned in a previous section, an inert granular bed was used in lieu of live propellant for this experiment. By using an inert bed, a post-test analysis of the igniter jet deposition can be performed. The bed consisted of soda-lime glass beads. The soda-lime glass beads conformed to Mil Spec G-9954A, and have a high degree of roundness as well as a small size distribution (with average diameters of 1.40 and 1.70 mm), similar to the live granular propellant. The beads do not react with the jet and can be used to visually determine the location of condensed-phase products as will be further discussed in the following sections. The method used to extract the data from the post test granular bed is described in section 4.5.3. An interchangeable flash-tube vent section with a single axial jet orifice was used for the deposition tests. The diameter of the orifice was varied by using multiple vent sections. One of these sections is shown in Figure 13. The condensed-phase deposition test rig is shown mounted on the test stand in Figure 14.

Figure 13: An interchangeable flash-tube vent section with an axial jet configuration used in the condensed-phase deposition experiments.
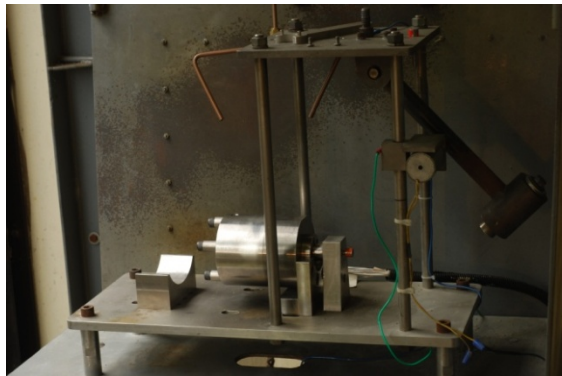
Figure 14: Condensed-phase deposition test rig configuration installed on test stand at HPCL.

4.5.1 Determination of Product Species from Black Powder Combustion

NASA's Chemical Equilibrium with Applications (CEA2) code (Gordon and McBride, 1994) was used to consider black-powder combustion products in the flash tube. The original composition of the black powder considered was charcoal (15.6 wt%), potassium nitrate (74.0 wt%), and sulfur (10.4 wt%)(ICT 2002). Table 1 shows the calculated product mass fractions for a constant-pressure combustor at several pressure levels, typical of those found inside the flash tube. The last column displays the calculated results from a constant-volume combustor consideration. It is evident from these results (both constant-pressure and constant-volume combustion cases) that a non-negligible percentage of the product species are in the condensed phase.

The condensed phase products in black powder combustion are shown to be 14 and 19% of products on a molar basis. In both constant volume and constant pressure analyses, all of the condensed-phase products are potassium-containing species. Since black powder is the only element of the experimental system where potassium exists before the igniter jet firing, the presence of potassium can therefore be used as an indicator of the presence of condensed-phase products.

13

Table 1: The major product species (> 1%) of black-power combustion from a constant-pressure or constant-volume reactor. Some species did not occur in both analyses.

Product Species	Mass Fraction			
	Pressure = 10.34 MPa (1500 psi)	Pressure = 15.51 MPa (2250 psi)	Pressure = 25.85 MPa (3750 psi)	Specific Volume = 2.65×10^{-4} m^3/kg (0.265 cc/g)
CO	0.18957	0.18606	0.18278	0.17467
CO_2	0.22791	0.21935	0.21248	0.16802
H_2	0.01514	0.01572	0.01613	0.01492
H_2O	0.10151	0.10515	0.10770	0.09194
H_2S	--	--	--	0.01665
KOH	0.06687	0.05873	0.05266	0.03465
N_2	0.18238	0.18445	0.18617	0.19037
S_2	0.01058	0.01331	0.01584	0.05073
S_2O	--	--	--	0.05073
KOH(l)	--	--	--	0.04446
K_2CO_3(l)	0.05698	0.07382	0.08787	0.03414
K_2S(l)	0.05394	0.04848	0.04338	--
K_2SO_4(l)	0.03143	0.02720	0.02369	--

4.5.2 Examination of Particles using Energy Dispersive Spectroscopy

Since potassium is not present in any of the granular bed materials before the igniter is fired, an elemental analysis can provide useful information about the location of the condensed-phase product deposition from the black-powder igniter jet. A total of 5 cases were analyzed on a Scanning Electron Microscope with Energy Dispersive Spectroscopy: a) an unburned black-powder pellet, b) an inert glass bead, c) an inert glass bead without visible products, and d and e) inert glass beads with visible products (items c, d, and e are shown in Figure 15). The resulting EDS analyses are shown in Figure 16.
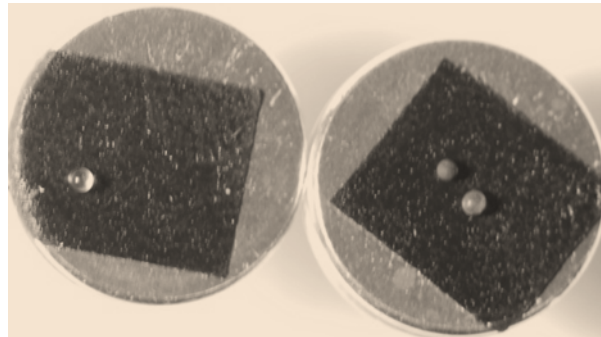

Figure 15: Glass beads after an igniter firing mounted for SEM analysis. The particles on the right hand side are covered with condensed-phase igniter products.

The analysis for the control samples (i.e. unburned) shows a high concentration of potassium on the black-powder specimen and no potassium on the inert particle. From the post-firing inert propellant bed, the particles that show visible products from the igniter firing have high concentrations of potassium relative to their concentration of oxygen that was present in all tests. The particles without visible products show no potassium. Some of the inert beads showed high concentrations of carbon. This was most likely due to the sodium carbonate used in the fabrication of soda-lime glass, and possibly the carbon mounting tape that the samples were on if the magnification of the analysis brought the mounting tape into focus.
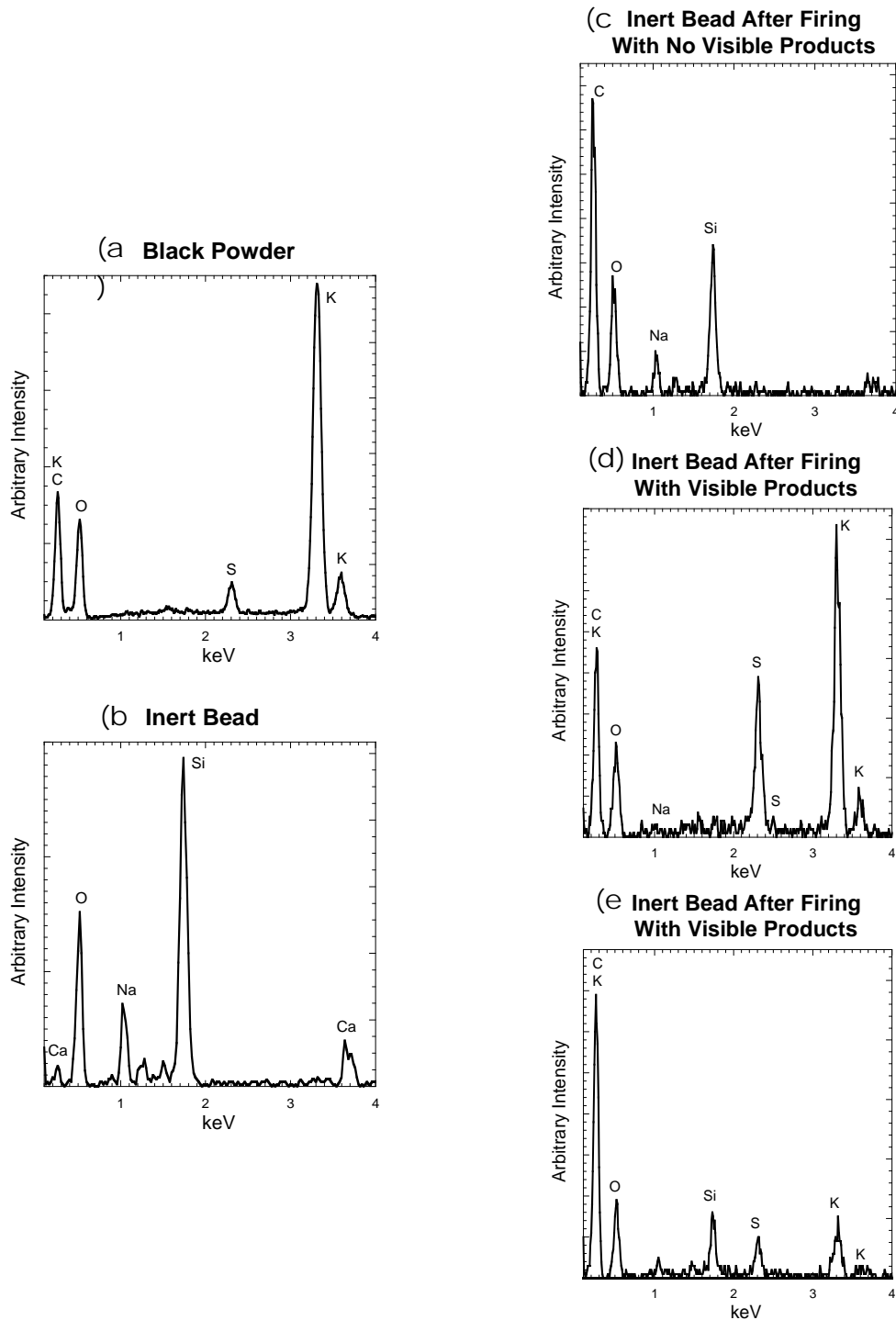
Figure 16: Energy spectra from SEM analysis cases. The two inert particle cases with visible products were located at different distances from the igniter jet orifice.

This analysis of the inert propellant shows that the dark condensed-phase products contain the potassium species that are only present in the black-powder pellet. These potassium species originate from the condensed-phase product species of the black-powder combustion.

16

SEM images in Figure 17 show the comparison of un-coated versus coated particles under magnification. The image of the particle coated with condensed-phase products indicates some non-uniformity in the amount of coverage of the deposition on the particle.
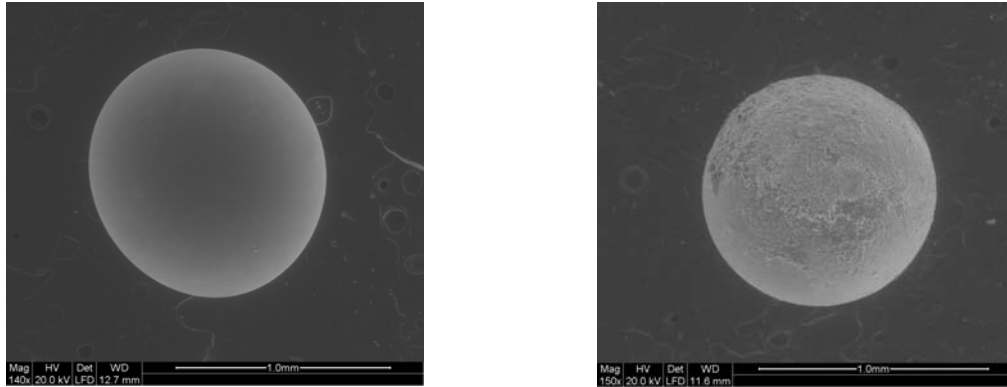
Figure 17: SEM images of two inert spherical particles at 150× magnification. Left: no visible condensed-phase products, right: a particle that is coated with condensed-phase products.

4.5.3 Determination of Location of Condensed-Phase Products from Black-Powder Combustion

In order to determine the domain of the coated region, a post-firing granular bed was extracted, layer-by-layer, with adhesive tape, and photographed (Figure 18). LABVIEW's NI Vision 8.6 software was used to analyze the photographs and determine the coated domain of the granular bed. The key steps of image analysis are shown in Figure 19.

Figure 18: Series of removed inert layers, the top left is closest to the orifice.
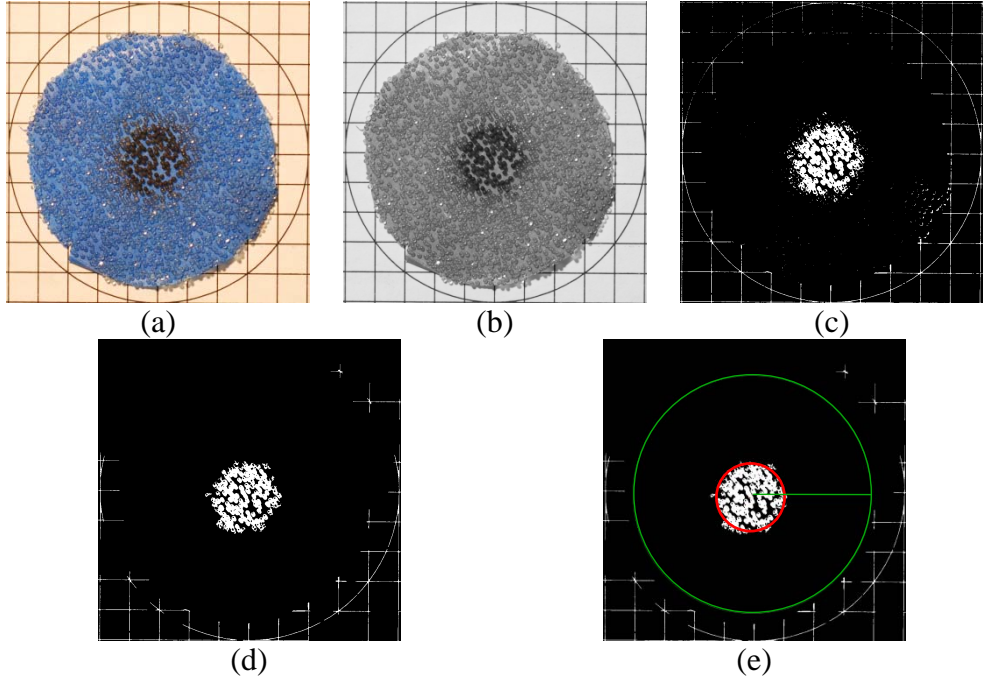
Figure 19: Stepwise analysis of coated region on a single layer of the inert granular bed. a) Original image, b) image changed to grayscale, c) intensity threshold applied to remove light colored particles, d) small-scale artifacts are removed, e) circle finder is used to find the diameter coated domain.

This method makes two key assumptions. First, the jet acts axisymmetrically. This is likely because the exit vent hole is round and gravity is unlikely to affect the high speed flow which only penetrates a short distance. Second, a binary system is created; particles are either covered with condensed phase products or not. Even a partially coated particle with the uncoated portion facing the camera is identified by the software as a coated particle because of the transparent nature of the glass beads.

5. Results

5.1 Igniter Characterization

The first pyrotechnic component of the ignition train is a percussion primer. Figure 20a shows the pressure-time traces of the head end section for the combustion of the primer alone. The traces show a high degree of repeatability. The variation in time delay between various firings is attributed to the mechanical components of the system as the zero-time signal is created by the mechanical action of the hammer impacting the firing pin. The same set of traces is shown again in Figure 20b with the curves aligned by their first pressure rise. With the pressure-time traces aligned in this manner, the similarity between each firing is more clearly seen.
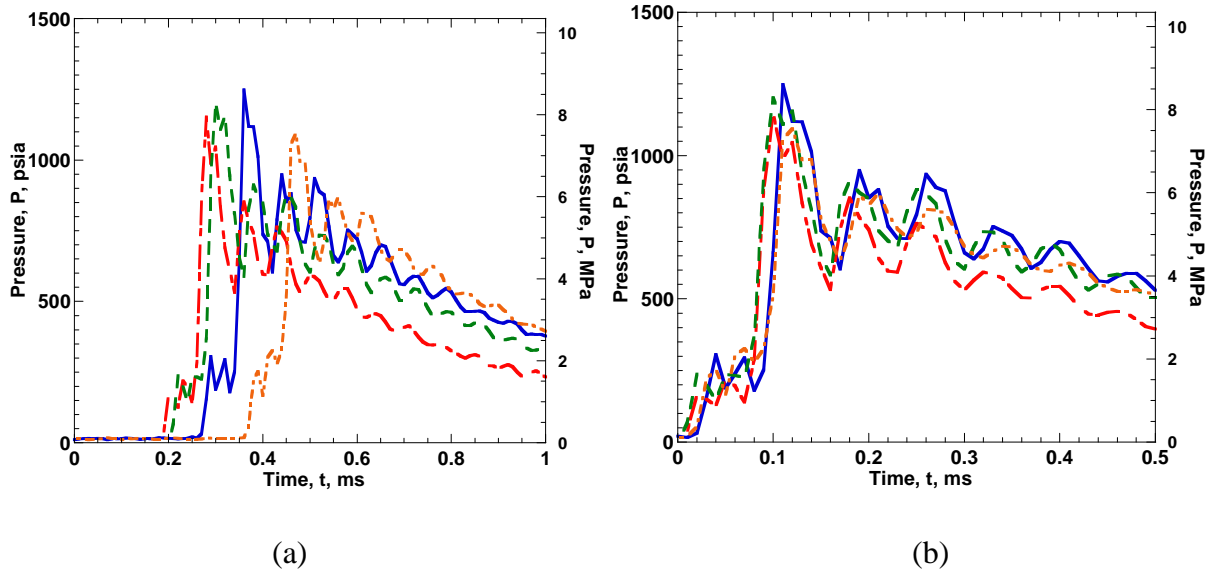
Figure 20: Pressure-time traces for 4 primer firings through a single, axial, vent hole with an orifice diameter of 1.65 mm. Traces aligned based on: a) trigger signal, b) first pressure rise

After the independent characterization of the percussion primer, a black-powder pellet was added to the ignition train in order to characterize a more typical igniter jet. The pressure-time traces for these firings are shown in Figures 21a and 21b. The characteristics of the primer's pressure-time history are absorbed into the overriding pressure of the black-powder combustion. This suggests that the black-powder combustion event is very rapidly initiated by the percussion primer. It is likely that the initial products from the primer, as opposed to the increase in pressure or the bulk products, cause the black powder to ignite. This is supported by the fact that black powder excels at burning in ambient conditions and a high percentage of the products from the primer combustion are in the solid phase. The significant variation between individual pressure curves is due to the burning characteristics of the black powder. Again, the misalignment of rise times is likely associated with a mechanical delay mechanism, but the curves still show some differences in their shapes and peak values when aligned by their first discernable pressure rise. A difference in peak value of approximately 3.4 MPa is shown by the pressure-time traces. Some curves show a sharp peak while others show a period of neutral burning. These pressure-time traces accurately represent the igniter jet behavior for the azimuthal flame spreading and the condensed phase-deposition experiments. High-speed photographic images of the igniter jet characterization tests are shown in Figure 22. The images show the under-expanded supersonic gas jet freely expanding into the quiescent air.
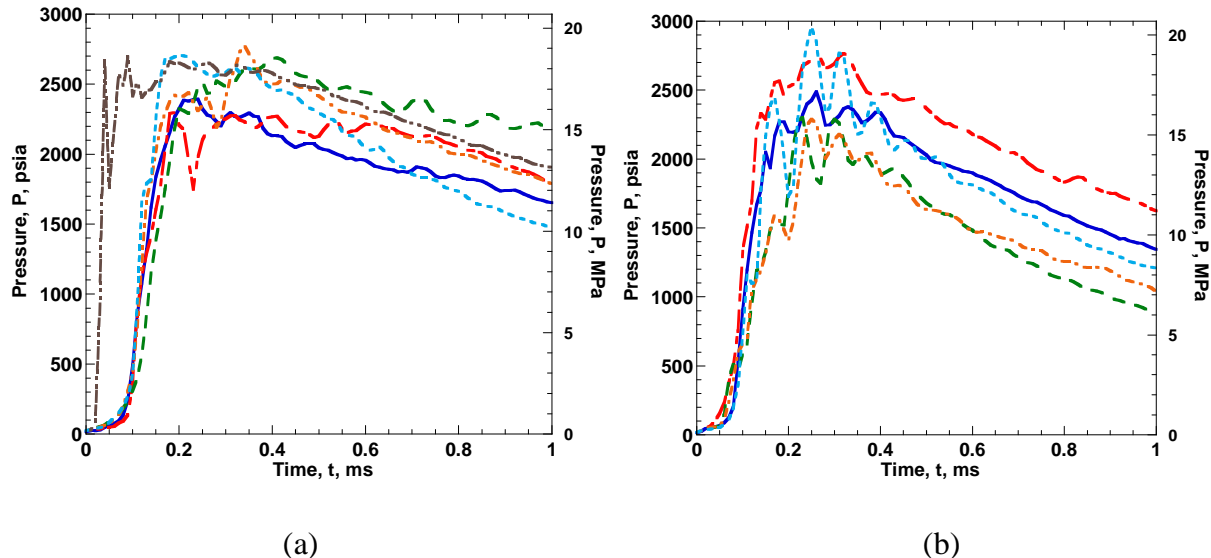
Figure 21: Pressure-time traces for 5 igniter jet firings through a single, axial, vent hole.
Orifice Diameter of: a) 1.65 mm and b) 1.85 mm.
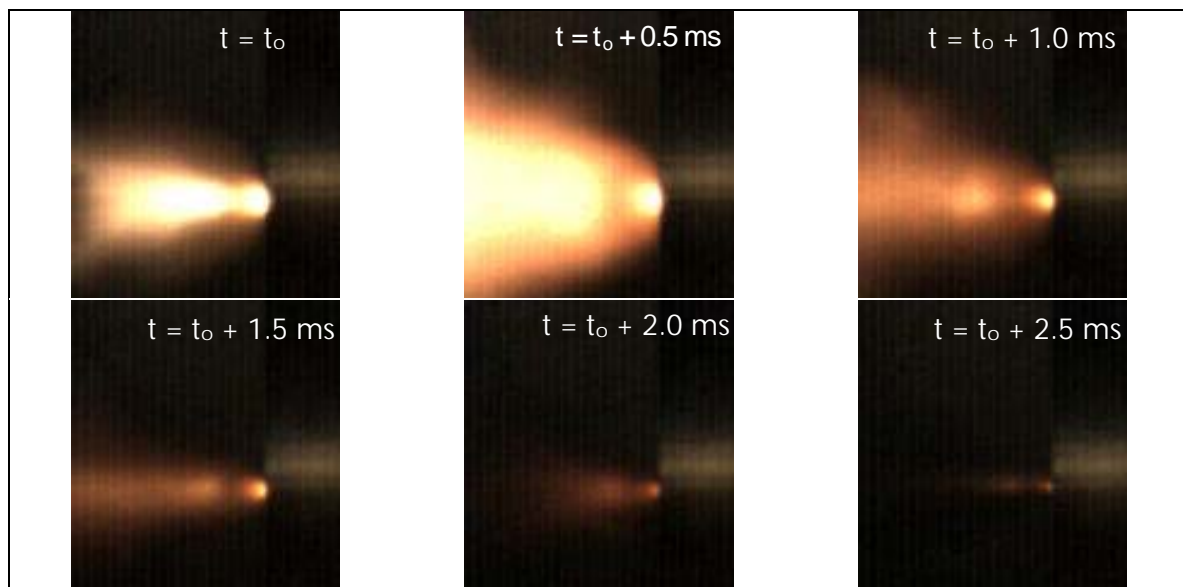
Figure 22: High-speed photography (2000 fps) of a single black powder jet leaving a 1.65 mm
diameter axial orifice into quiescent air.

     The igniter-jet discharge from the interchangeable flash-tube vent section used for the axial flame-spreading experiments exhibited different behavior from the pressure-time traces shown above. The characteristic pressure-time traces are shown in Figure 23. The curves show much less repeatability than the axial cases. This is most likely due to the more complex flow associated with the turning of the jet.
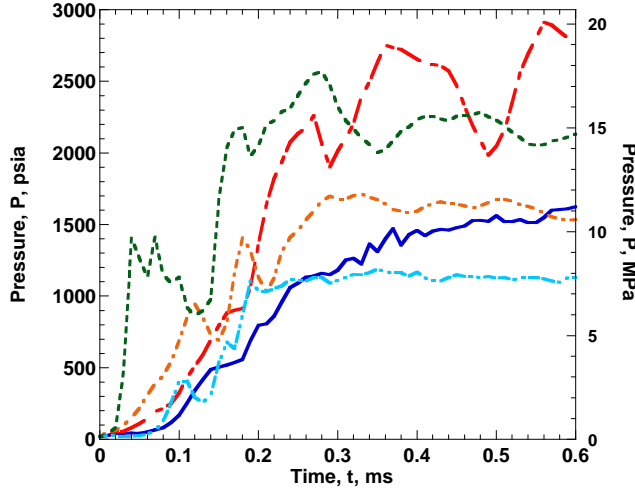
Figure 23: Pressure-time traces for 5 igniter jet firings through the axial flame-spreading interchangeable flash-tube vent section (four radial vent holes).

5.2 Azimuthal Flame Spreading

5.2.1 Gas Penetration in Inert Bed Firings

Radial igniter jets were fired into an inert bed of propellant simulant, while being viewed by a high-speed camera. As the granular bed does not react with the igniter jet (this was confirmed through pressure-time traces and post-test inspection), the high-speed photographic images correspond only to the visible products of the igniter jet. High-speed images (Figure 24) show that the igniter jets penetrate the bed to the chamber wall with nearly symmetric spread angles of approximately 70°. After reaching the wall, the hot gas slightly spreads azimuthally prior to its quenching.
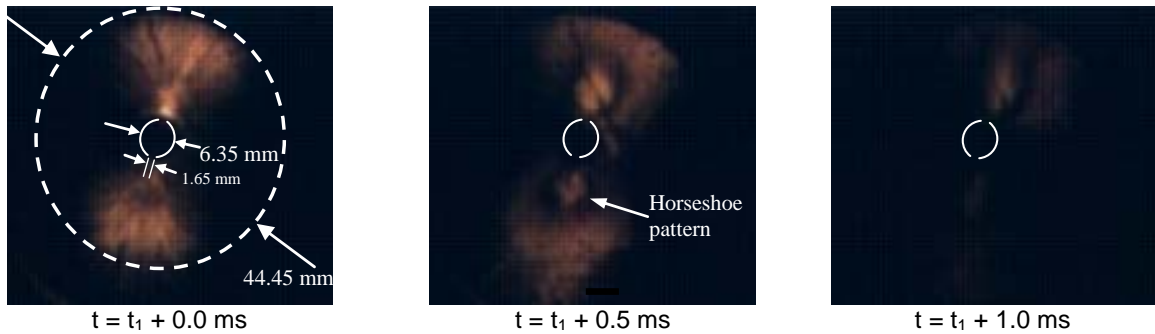
Figure 24: High-speed camera images of gas penetration of radial igniter jets into an inert bed (t_1 corresponds to the time of the first visible image).

21

The second frame shows a black horseshoe pattern. Upon post-test inspection this corresponds to the deposition of condensed-phase igniter products onto the sacrificial window. This pattern will also be seen in the azimuthal tests containing live propellant.

5.2.2 Radial Jet Firings with Granular Bed Partially Loaded with Live Propellant

The initial tests involving live propellant did not experience sustained combustion due to rapid depressurization, which was caused by the overly large area of the exit ports. The high-speed camera images that are shown in Figure 25 display evidence of combustion in the regions of the granular bed penetrated by the igniter jets. However, the pressure-time traces shown in Figure 26 confirm that combustion was not sustained (the only pressure transducer to read a significant rise in pressure was the one installed in the flash tube). The pressure-time traces from the test section effectively remained constant throughout the duration of the event.
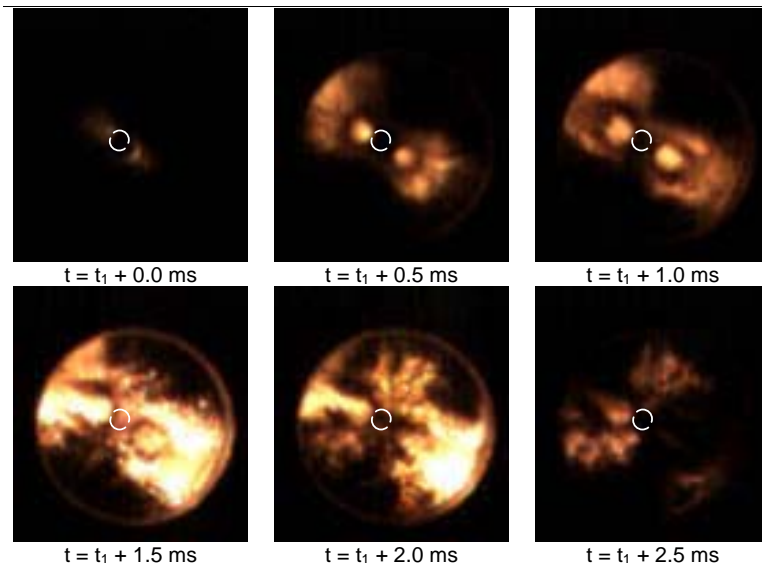
Figure 25: High-speed photographic images of localized burning of propellant in granular bed partially loaded with live propellant grains.
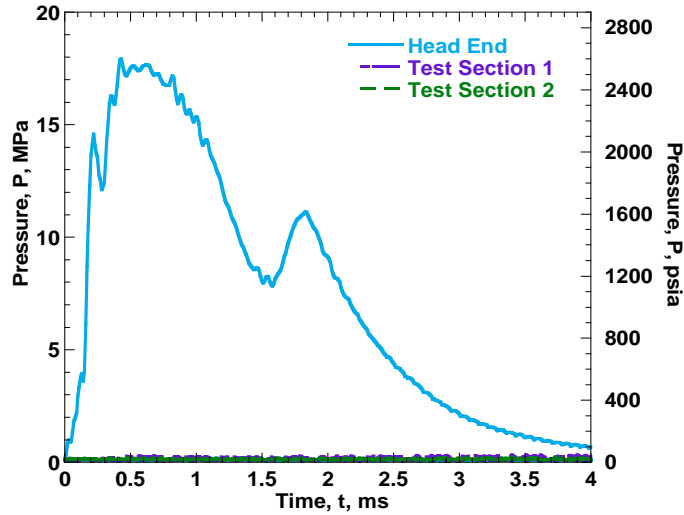
Figure 26: Pressure-time traces for granular bed partially loaded with live propellant grains.

To achieve sustained combustion, the area of the four axisymmetric exit ports was restricted by installing a metal strip, with a small hole punched in the center, over the paper burst disks for each exit port. Figure 27 shows the gas penetration of the igniter jets reaching the test chamber wall prior to ignition. It is also evident that rapid flame spreading has occurred. The pressure-time traces give a peak pressure of approximately 40 MPa at 5 ms after the initial pressure rise (Figure 28).
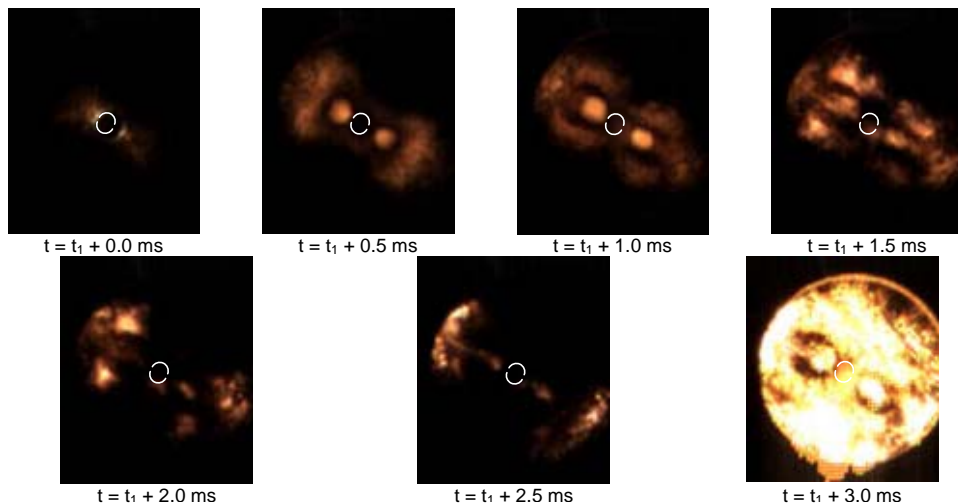
Figure 27: High-speed photographic images of ignition and sustained combustion of granular propellant bed with restricted exit ports.

23
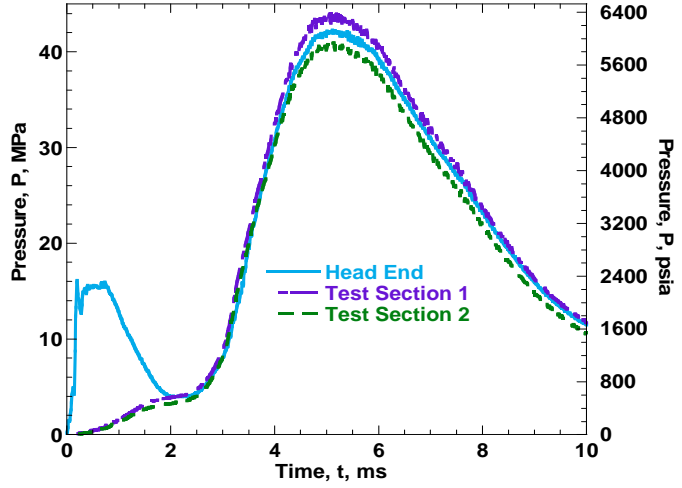
Figure 28: Pressure-time traces for test with sustained combustion of granular propellant bed with restricted exit ports.

These two figures also support additional observations. Firstly, as shown in the high-speed photographic images, the luminous gas penetration of the igniter jet reaches the chamber wall prior to any azimuthal flame spreading. Secondly, the pressure-time traces show that the pressure spike from the igniter jet is past its peak and has declined significantly prior to the overall ignition of the live propellants in the test chamber. This second observation is further supported by a comparison of the data from tests utilizing visible spectra photodetectors (Figure 29).
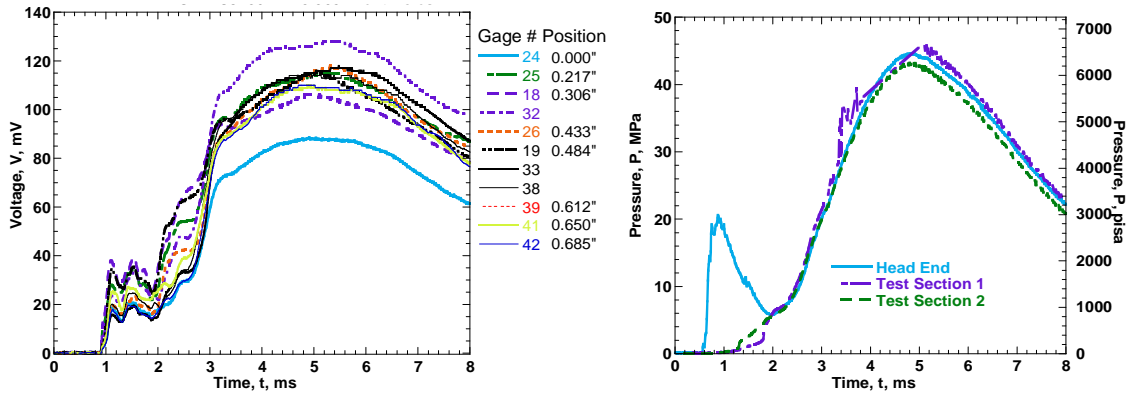
Figure 29: Visible-light intensity on left and pressure-time traces on right for combustion of granular propellant bed with restricted exit ports.

The two plots contained in Figure 29 share a common zero. One can see a dip in the visible-light intensity prior to a steep rise that corresponds in time to the initial merge of the head-end and test-section pressure-time traces, or in other words, to the onset of propellant ignition. This supports the observation that the igniter jet has fully penetrated the bed prior to ignition. The comparison is further shown in Figure 30, which superimposes pressure and visible-light data. The significance of this observation is that it validates the characterization of the igniter jet through the use of an inert granular bed. While the effect of propellant ignition

and flame spreading on the penetration and the deposition of condensed-phase products from the igniter jet is negligible, the conductive heat-transfer process induced by the condensed-phase product deposition has a strong influence on the ignition process of the granular solid propellant. This effect can be seen by examining the 5th and 6th images of Figure 27. When the gas penetration event is nearly complete (the propellant bed has limited luminous regions at t=2 to 2.5 ms, when the pressure-time traces merge), conductive heat transfer from deposited condensed-phase products continues to play a role prior to propellant ignition. Finally, the live propellant grains in the granular bed ignite and a very rapid flame spreading in the azimuthal directions occurs, leading to a highly luminous image in Figure 27.
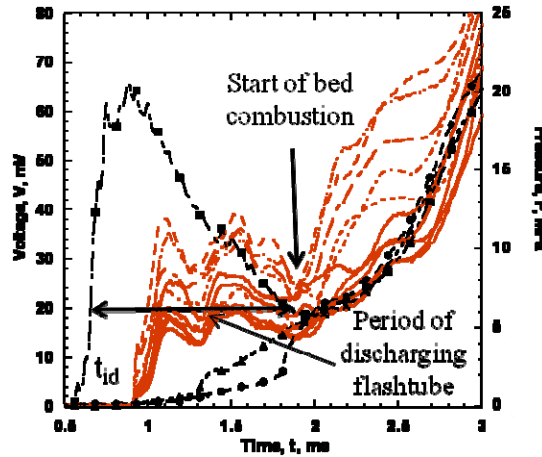
Figure 30: Visible-light intensity (red) overlaid with pressure-time trace (black) for combustion of granular propellant bed with restricted exit ports.

5.3 Axial Flame Spreading

5.3.1 High-Speed Camera Results

To get a qualitative assessment of flame spreading, the axial chamber configuration was run with a partial granular propellant bed loading and a high-speed camera. The overall propellant loading for this test was: the percussion primer, one centrally perforated black-powder pellet, and 3.0 grams of M48 ball propellant. The rest of the free volume was filled with inert propellant (the same simulant used for the condensed-phase deposition experiments) in order to keep the packing density similar to a volume completely filled with live propellant. The pressure-time traces are shown in Figure 31a. The depressurization indicates that the shear disk ruptured at about 2.0 ms. Later tests instrumented with photodetectors would implement a break-wire to confirm this depressurization time.

Four frames of a high-speed (2000 fps) movie were captured (Figure 31b). The live granular propellant only takes up a small fraction of the chamber volume, and the inert propellant is unlikely to significantly compress. This leads to the conclusion that the light emissions seen do not correspond to the burning surfaces. Instead they show the hot gasses produced by the igniter jet and the combustion of live propellant on the right hand side (upstream) moving through the interstitial spacing between inert granules in the first three images. This indicates

25

that when using the array of photodetectors, the visible light photodetectors will still receive a signal even when the hot gas front is not in close proximity to a burning surface. The final image corresponds to after the shear disk failure, and shows the rapid depressurization of the hot gases from the chamber.

(a)   (b)
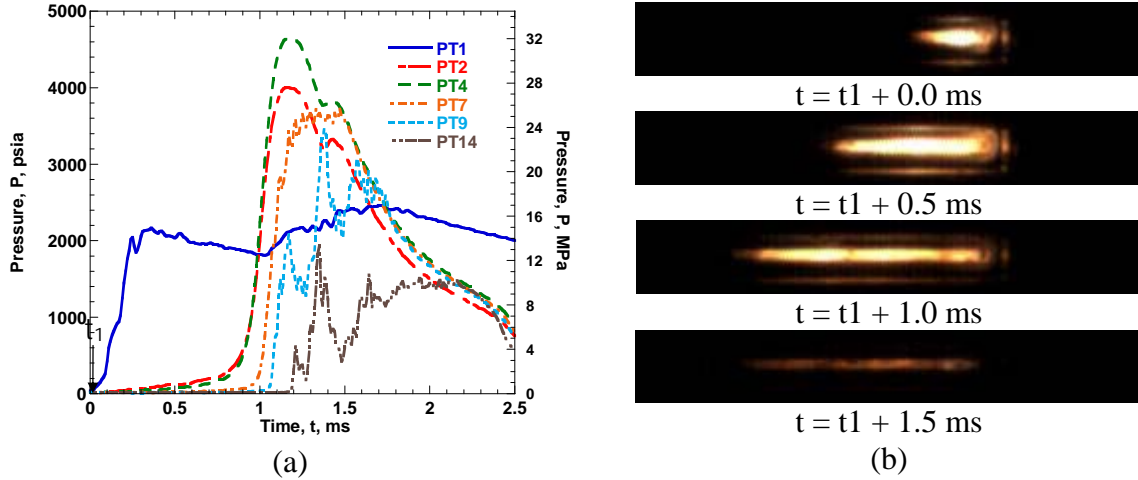
Figure 31: a) Pressure-time traces, and b) high-speed camera images of burning granular propellant in axial flame-spreading test rig. Flow is from right to left.

5.3.2 Comparison of Burning Surface and Hot Gas Fronts

The same propellant configuration as the previously discussed test (3.0 grams granular propellant upstream) was run with the photodetector array instead of the high-speed camera. The overall pressure-time and intensity-time plots are shown in Figure 32. Figure 33 shows more detailed views of the photodetector rises and corresponding pressure-time traces for the time period when the flame front passes location PT4 (2.78 cm downstream of head end).
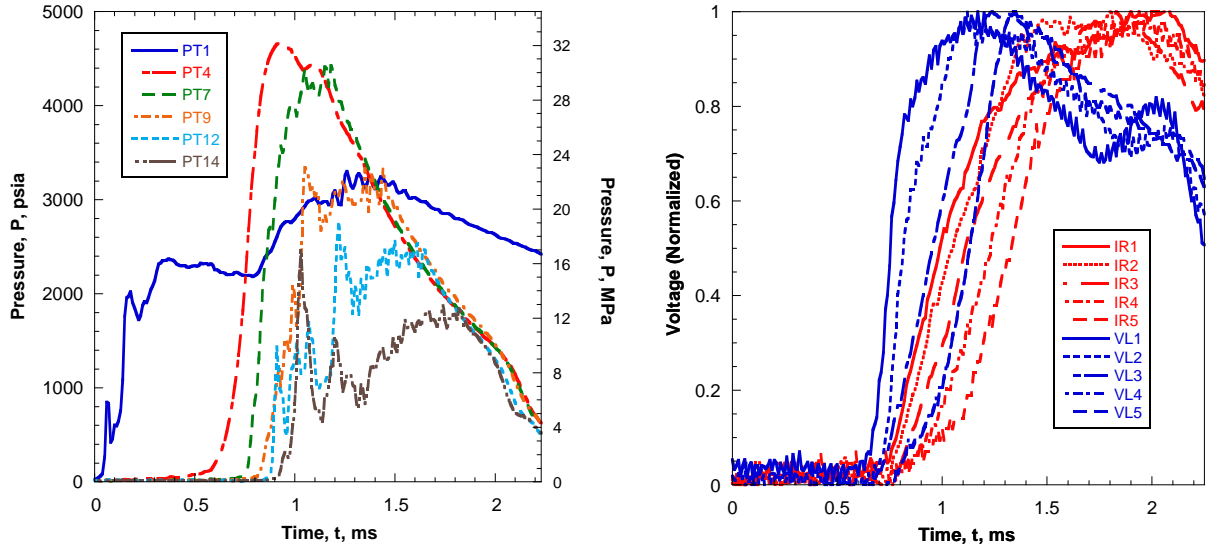
Figure 32: Axial chamber with 3.0 g of live granular propellant and remainder inert. Left: Pressure-time plot. Right: Intensity-time plot for both visible (blue) and infrared light (red) photodetectors.
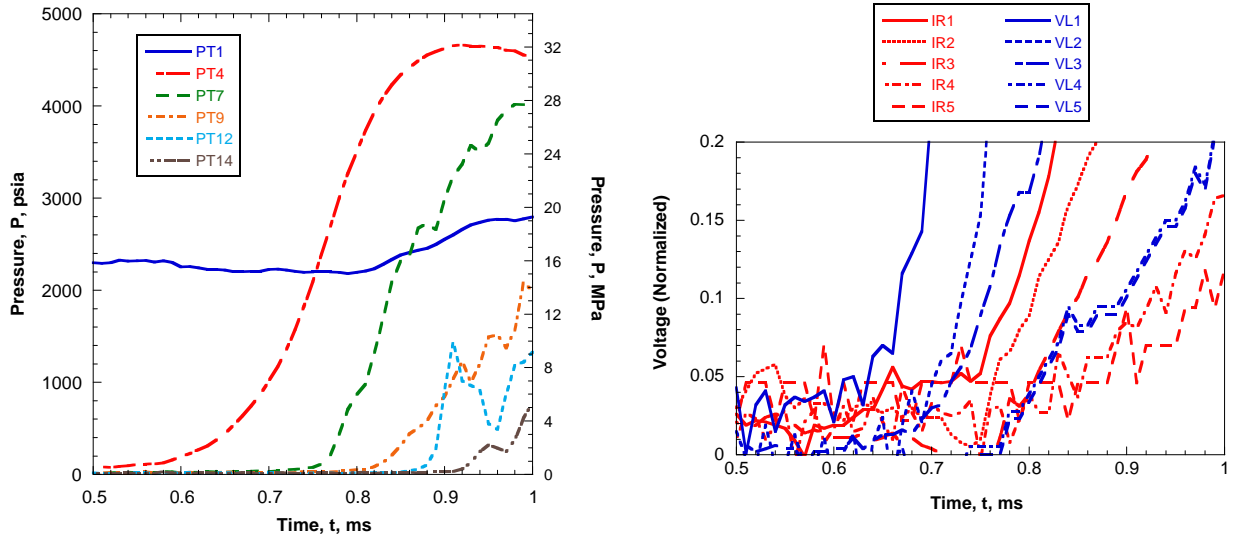
Figure 33: Expanded pressure-time and light intensity-time traces showing flame front passage in front of PT4.

The live propellant was placed upstream, in front of photodetector stations 1 and 2, and pressure transducer location PT 4. The flame front trails the hot gas front by 0.12 ms at stations 1 and 2 as determined by the time when each signal passes 20% of its peak value. Photodetectors at stations 4 and 5 show some discretization noise as they were recorded on a different DAQ with lower bit resolution. In 4 different tests, with peak pressures between 28 MPa and 41 MPa the hot gas and flame front showed an average separation of 0.15 ms. These tests only go to 25% of the design value for the pressure of the system; higher propellant loadings can be achieved which will place the live propellant in front of the other photodetector stations providing more flame-spreading data and increased maximum chamber pressure.

27

The first rise of photodetectors at station 1 is again after the action of the igniter jet. However, in this set-up, the photodetectors do not have line-of-sight assessment of the igniter jet. This again points to the igniter jet penetrating the bed before intense burning begins.

5.4 Condensed-Phase Deposition in Inert Granular Bed Firings

Axial igniter jets were fired into an inert bed of glass beads using the experimental setup discussed in Section 3.3. The following factors were systematically varied during testing: particle diameter, orifice diameter, and propellant mass.

For comparison, a primer jet was fired into an inert propellant bed. The depth of penetration was defined by the depth to the first layer of the granular bed where there were no visible condensed-phase products. The profiles of the coated regions for two separate tests (with different jet-orifice diameters) are shown in Figure 34. The boundaries of the coated regions expand radially from the orifice (located at the origin) and then decreases in radius as the axial distance increases.
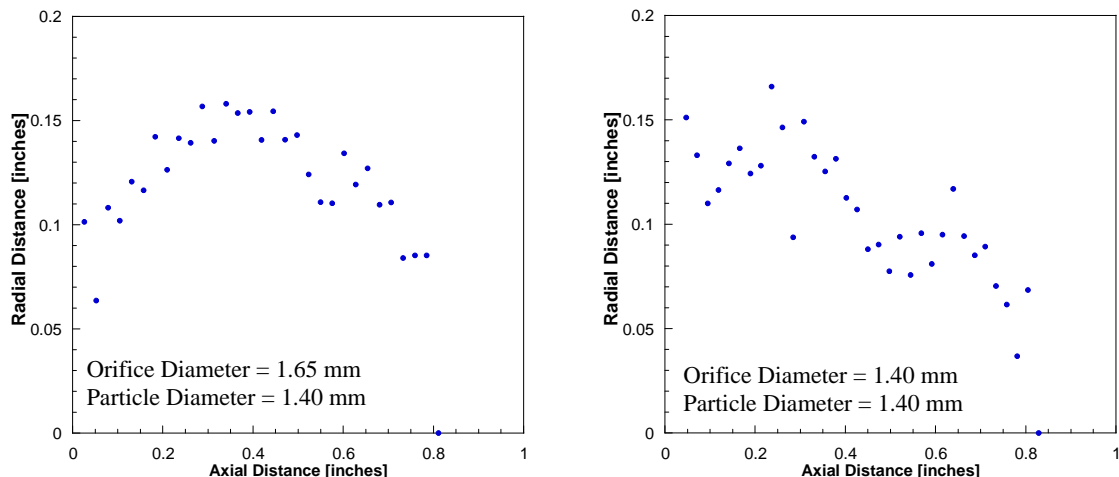
Figure 34: Two typical profiles of condensed-phase deposition for percussion-primer jets (igniter jets without any black-powder pellets in the flash tube) fired into inert granular beds.

Two typical boundaries of the coated region in the granular bed by condensed-phase products are shown in Figure 35. These boundaries were made with the standard igniter jet that included both a percussion primer and black-powder pellets. It is interesting to note that while the depths of penetration in these two plots do not vary significantly from those given in Figure 34; the penetration boundary in the radial direction from the axial jet discharge is much broader than the percussion primer alone.

Due to the fact that the igniter jet is highly transient, the shape of the boundary of the coated region does not have the same form as a conventional steady-state supersonic gas jet profile. From the measured boundary of the coated region, one can visualize that the jet must expand abruptly at the jet-orifice exit plane; this causes the deepest radial penetration depth near the exit from the initially highly under-expanded jet. Immediately after the jet expansion the radial depth of the boundary of the coated region remains relatively constant. This is followed by a steep drop in radial penetration as axial distance increases. This sharp decrease is believed

28

to be caused by the interception of condensed-phase products by the spherical inert grains. The gas phase products can still penetrate the interstitial voids to a greater depth, but the condensed-phase liquid droplets were unable to navigate the tortuous passage through the granular bed.
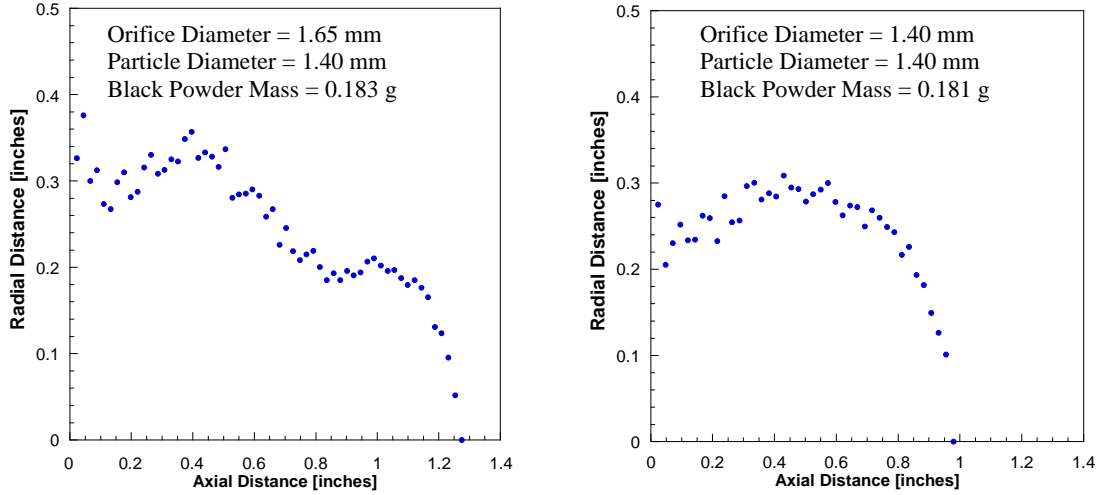
Figure 35: Two typical boundaries of condensed-phase product deposition from the combination of the percussion-primer and black-powder pellets into an inert granular bed.

A correlation for the depth of penetration of the condensed-phase products into the granular bed was found in the following form:

$$\frac{L}{d_{jet}} = 9.361 \times 10^3 \left(\text{Re}_{d_{jet}} \right)^{-1.99} \left(\frac{\bar{P}}{P_{atm}} \right)^{1.86} \left(\frac{d_{part}}{d_{jet}} \right)^{-0.55} \tag{1}$$

The first term is the Reynolds number based on the jet properties at the igniter jet orifice, and is defined as: $\text{Re}_{d_{jet}} = \rho_{jet} U_o d_{jet} / \mu_{jet}$. The flow is assumed to be an ideal gas with gas properties calculated from NASA-CEA code. The average measured pressure was determined by integrating the pressure from the first recorded rise to subsequent decay down to 3.45 MPa (500 psia). The correlation is shown in Figure 36 with measured values plotted against calculated values. The error bounds shown are at $\pm 30\%$, which is consistent with Yang and Keairns (1979). The error bars are at $\pm$ one layer of inert propellant. The outliers are likely due to the non-reproducibility of black-powder combustion and the complex flow dynamics that are not completely described by the non-dimensional parameters given.

This correlation gives three important relationships. As the value of $\text{Re}_{d_{jet}}$ increases, the condensed-phase deposition on adjacent particles increases, which lowers the jet's ability to penetrate further into the bed. This is shown by the negative exponent on $\text{Re}_{d_{jet}}$ in Eq. (1). An increased average pressure is analogous to an increased driving force for jet penetration, and results in higher depth of penetration. Finally, as the particle diameter increases, the extent to which the condensed-phase products are diverted from the axial direction increases, this decreases the depth of penetration.
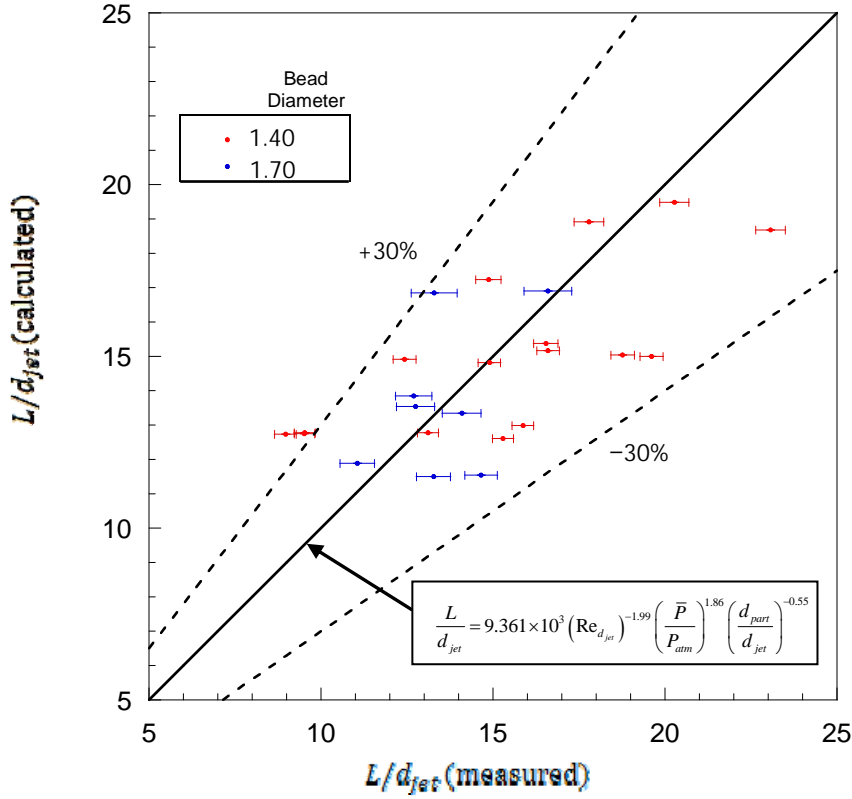
Figure 36: Plot of correlation for calculated versus measured depth of penetration of condensed-phase products into a granular bed.

The boundary of the region of the granular bed coated with condensed-phase products was used to create a correlation for the ratio of the volume of that coated region to the volume of a single inert particle. The correlation was found using the same non-dimensional parameters as the L/d_{jet} correlation:

$$\frac{V_{\text{covered}}}{V_{part}} = 1.958 \times 10^5 \left(\text{Re}_{d_{jet}} \right)^{-1.94} \left(\frac{\bar{P}}{P_{atm}} \right)^{2.18} \left(\frac{d_{part}}{d_{jet}} \right)^{-1.28} \tag{2}$$

This is plotted in Figure 37. The error bounds for the volume measurement are due to error in measuring the radius of condensed-phase deposition before calculation of volume. Again as the Reynolds number increases the condensed-phase deposition to adjacent particles increases, which decreases the outer boundary of the volume affected by the jet. Therefore, the exponent for the Reynolds number in Eq. (2) is negative. The average pressure again acts as a driving force to increase the volume covered. Finally, as the particle diameter increases, the tortuosity of the passage for the combustion products to travel through increases, this causes a higher rate of deposition in the vicinity of the igniter-jet exit plane. Thus, the volume containing the coated particles decreases.
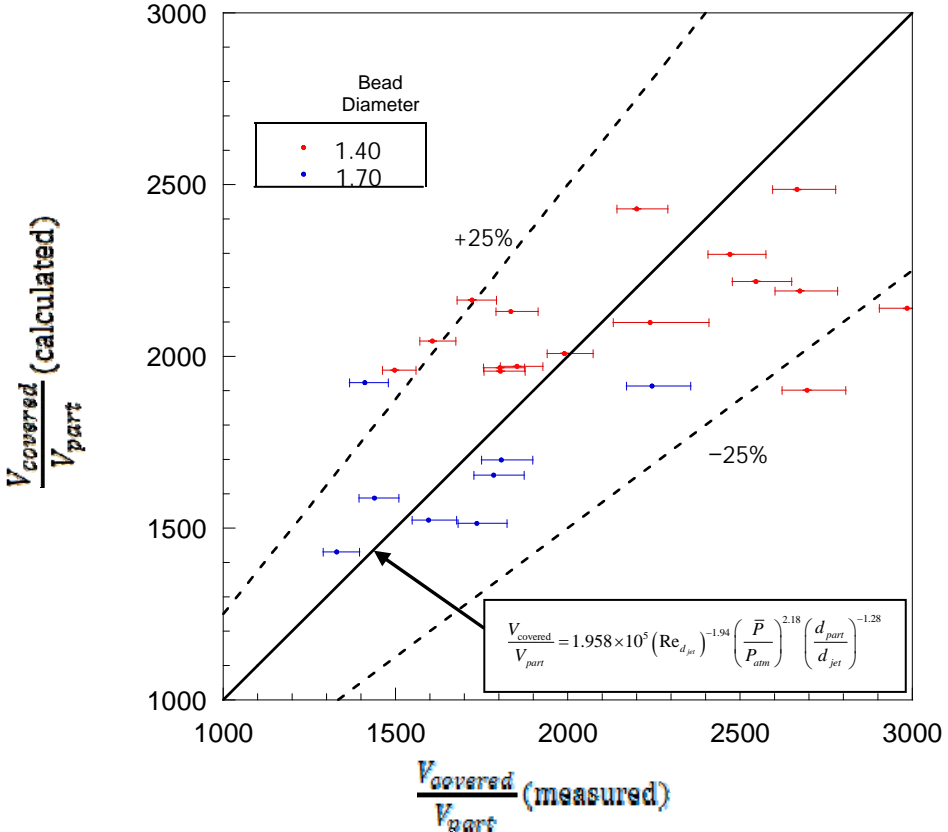
Figure 37: Plot of correlation for calculated versus measured volume of the coated region.

Finally, a correlation was created for the maximum radial spread of condensed-phase products from the jet. Again the same non-dimensional parameters were used.

$$\frac{d_{cond,max}}{d_{jet}} = 1.218 \times 10^3 \left(Re_{d_{jet}} \right)^{-0.44} \left(\frac{\bar{P}}{P_{atm}} \right)^{0.37} \left(\frac{d_{part}}{d_{jet}} \right)^{0.74} \tag{3}$$

This is plotted in Figure 38. The same relationship holds for the Reynolds number as in the previous correlations. That is, as the Reynolds number increases, there is increased deposition in the close vicinity of the igniter-jet exit, and the radial penetration decreases. This is again referenced by the negative exponent in Eq. (3). As the average pressure increases, the degree of under-expansion of the jet increases and thus the radial penetration increases. As the average diameter of the particles in the bed increases, the tortuosity of the passage for the product jet increases, and therefore, the radial penetration increases.

31
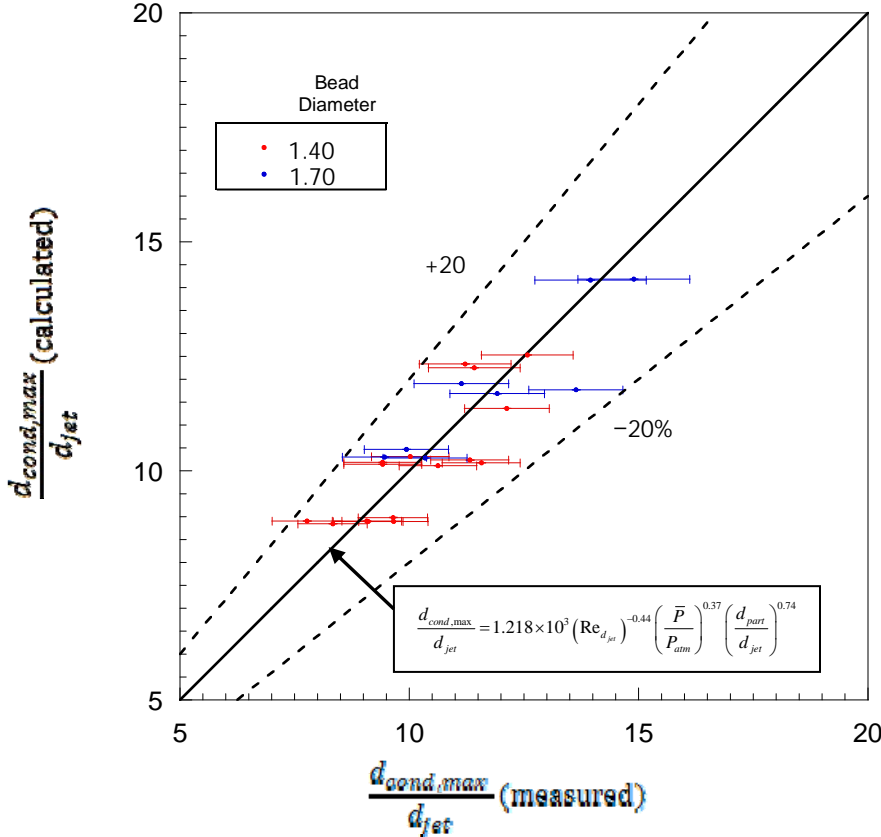
Figure 38: Plot of the ratio of calculated versus measured maximum radial penetration of condensed phase deposition to jet diameter.

6. Conclusions

The fundamental ignition processes of a granular propellant bed were studied. The first stage of ignition consists of a percussion primer and black-powder igniter jet impinging onto a granular propellant bed. High-speed photographic images and data from visible-light photodetectors confirm that the igniter jets used in the azimuthal configuration fully penetrate the bed prior to the ignition of the granular propellant. This finding allows the modeler to consider the igniter-jet penetration and the deposition of condensed-phase products as an independent process prior to the onset of ignition of the propellant grains and subsequent flame-spreading in the granular solid-propellant bed.

The axial configuration shows that the simultaneous measurement of pressure, visible, and infrared light signals can be measured from a burning granular propellant bed. At chamber pressures ranging from 28 – 41 MPa the hot gas and burning surface fronts were separated by approximately 0.15 ms. Further tests at up to 138 MPa can be conducted to find a functional relationship between these fronts and flow parameters.

NASA-CEA code calculations for a constant-pressure and constant-volume reactor determine that the condensed-phase species in black-powder combustion make up 10 to 20 wt% of the total products in the discharging jet. The most likely species of condensed-phase products contained in the jet are KOH, K_2CO_3, K_2S, and K_2SO_4. The presence of these elements (except

H) was confirmed via EDS on inert particles coated with condensed-phase products. This information was used to determine the extent of the coated region within the granular bed.

Multiple layer analysis of inert granular beds, fired onto by an igniter jets, allowed for the development of three correlations which describe axial depth, affected volume, and maximum radial penetration of the condensed-phase deposition by the igniter jet. These correlations relate operating parameters to the measured geometric dimensions of interest to within 30% or better. These correlations can be utilized for modeling and simulation work in the interior ballistics of ballistic propulsion systems.

7. Acknowledgements

8. References

Asay, B. W., S. F. Son, and J. B. Bdzil. "The role of gas permeation in convective burning." Int. J. Multiphase Flow 22.5 (1996): 923-952

Williams, A. W., Brant, A. L., Kaste, P. J., Colburn J. W., (September 2006) *Experimental Studies of the No. 41 Primer and Ignition of 5.56-mm Ammunition*, Army Research Laboratory, ARL-TR-3922.

Kooker, Douglas E., Lang-Mann Chang, and Stephen L. Howard. "Flamespreading in Granular Solid Propellant: Design of an Experiment." Army Research Laboratory, 1993: ARL-MR-80.

Acharya, R. and Kuo, K. K., (April 2007) Finite Element Simulation of Interior Ballistic Processes in 120-mm Mortar System, F. Galvez and V. Sanchez-Galvez, Eds, *23rd International Symposium on Ballistics* Vol. 1, pp. 343-350.

Porterie, B. and Loraud, J.C., (June 1994) An investigation of interior ballistics ignition phase, *Shockwaves*.

Gordon, S. and McBride, B. J., (1994) *Computer Program for Calculation of Complex Chemical Equilibrium Compositions and Applications I. Analysis*, NASA Reference Publication 1311.

Anon, ICT Thermochemical Database, Institute of Chemical Technology, Pfinztal, Germany, 2002.

Yang, W. C., and Keairns, D. L., (1979) *Estimating Jet Penetration Depth of Multiple Vertical Grid Jets*, Industrial and Engineering Chemistry Fundamentals 18, No. 4, pp. 317-319.

Appendix A

Properties of Ignition Train Elements

Table A1: Primer Specifications

Make	Federal No. 150 large pistol primer
Type	Percussion primer
Dimensions	Height: 0.121″
	Diameter: 0.210″
Weight of charge	35mg

Table A2: Black Powder (MIL-A-2250) Specifications

Chemical Composition	Potassium Nitrate	74.0% $\pm$ 1.0
	Sulfur	15.6% $\pm$ 1.0
	Charcoal	10.4% $\pm$ 1.0
Dimensions	Length: 0.228″	
	Outside Diameter: 0.202″	
	Central Perforation Diameter: 0.047″	
Specific Gravity	1.70 $\pm$ 0.05	

Table A3: Granular Propellant Physical Characteristics (M48 Ball Propellant)

Description	Value
Initial bed porosity	0.407
Initial radius of the solid propellant grain	0.0545 cm
Molecular weight of the solid propellant gas	56 g/gmole
Density of propellant	1.55 g/cm^3
Ablation temperature of the solid propellant	525 K
Ignition temperature of the solid propellant	600 K
Density of liquid products of combustion from flash tube	8.45 gm/cc
Specific heat of liquid products of combustion from flash tube	0.031 cal/gm-K
Thermal conductivity of liquid products of combustion from flash tube	0.000205 cal/cm-s-K
Thermal conductivity of M48 ball propellant	0.0005998 cal/cm-s-K
Specific heat of M48 ball propellant	0.35 cal/gm-K
Thermal diffusivity of M48 ball propellant	0.0011045 cm^2/s
Adiabatic flame temperature of BP	1930 K
Emissivity of the propellant	1
Adiabatic flame temperature of solid propellant (K)	2831

Appendix B

CEA Analysis of Black Powder Combustion Products

Combustion (Enthalpy and Pressure) Analysis

Input

```
problem
        hp
        p,atm= 150, 200, 250, t,k=3800

react
        name=K1NO3     K 1 N 1 O 3                          h,kj/mol=-494.63        t,k=298.15
wt%=74
        name=Sulfur S 1                                     h,kj/mol=0              t,k=298.15
wt%=10.4
        name=charcoal     C 10 CA .009 H 6.696 O 2.2117     h,kj/mol=206.69         t,k=298.15
wt%=15.6
end

output   siunits
         short
         massf
         transport
```

Tabulated Output

Table B1: CEA output for constant pressure combustion of black powder (mole fractions below 1% omitted)

Species	Mass Fraction		
	Pressure = 1500 psi	Pressure = 2250 psi	Pressure = 3750 psi
CO	0.18957	0.18606	0.18278
CO_2	0.22791	0.21935	0.21248
H_2	0.01514	0.01572	0.01613
H_2O	0.10151	0.10515	0.10770
KOH	0.06687	0.05873	0.05266
N_2	0.18238	0.18445	0.18617
S_2	0.01058	0.01331	0.01584
$K_2CO_3(l)$	0.05698	0.07382	0.08787
$K_2S(l)$	0.05394	0.04848	0.04338
$K_2SO_4(l)$	0.03143	0.02720	0.02369
Temperature (K)	2293	2323	2345
Average Molecular Weight of Product Species	49.839	50.406	50.876
Ratio of Specific Heat	1.0789	1.0714	1.0653

Combustion (Internal Energy and Volume) Analysis

Input

problem
        uv   rho,g/cc=0.265, t,k=3800

react
        name=KNO3   K 1 N 1 O 3   h,kj/mol=-494.63   t,k=298.15   wt%=74
        name=Sulfur S 1   h,kj/mol=0   t,k=298.15
wt%=10.4

38

name=charcoal   C 10 CA .009 H 6.696 O 2.2117   h,kj/mol=206.69   t,k=298.15
wt%=15.6
end

Tabulated Output

Table B2: CEA output for constant volume combustion of black powder (mole fractions below 1% omitted)

Species	Mass Fraction Specific Volume = 0.265 g/cc
CO	0.17467
CO_2	0.16802
H_2	0.01492
H_2O	0.09194
H_2S	0.01665
KOH	0.03465
N_2	0.19037
S_2	0.05073
S_2O	0.05073
KOH(l)	0.04446
K_2CO_3(l)	0.03414
Temperature (K)	2577
Average Molecular Weight of Product Species	52.033
Ratio of Specific Heat	1.0451
Pressure (bar)	881.34

Appendix C

Important Chamber Dimensions

Table C1: Radial/Azimuthal Test Rig Configuration Dimensions

Item	Location/Size (inches)	Note
Axial flashtube		
Length	1.855	From primer to end of vent-hole
Axial vent diameter	0.055, 0.0595, 0.065, 0.073	Four separate parts
Radial flashtube		
Length	2.385	From primer cup to vent holes
Diameter	2 x 0.065	Offset 180°
PT 1	0.956	From primer
Main chamber		
PT 2-5	0.288	From start of bed, Centered in test chamber
Volume	1.3830	in^3
Length	0.575	
Chamber	1.750	
Photodetector offset	0.217	Offset in both x and y from center to form a grid

Table C2: Axial Test Rig Configuration Dimensions

Item	Location/Size (inches)	Note
Length of radial flashtube	2.600	From primer to center of vent-holes
Vent diameter	4 x 0.040	Axi-symmetric
Length of chamber	4.575	
Diameter of chamber	0.700	
Length of window	0.330	
Start of window	0.877	Measured from start of chamber, matches radial vent-hole location
PT 2-3	0.365	"
PT 4-6	1.094	"
PT 7-8	1.823	"
PT 9-11	2.552	"
PT 12-13	3.281	"
PT 14-16	4.011	"
PD 1	0.915	"
PD 2	1.146	"
PD 3	1.377	"
PD 4	1.607	"
PD 5	1.838	"
PD 6	2.069	"
PD 7	2.300	"
PD 8	2.531	"
PD 9	2.761	"
PD 10	2.992	"
PD 11	3.223	"
PD 12	3.454	"
PD 13	3.685	"
PD 14	3.915	"
Shear Disk Diameter	1.250	1.25 nominal, can range from 1 1/8 - 1.344

Appendix D

Inert Bed Firing Tests

Table D1: Test matrix and derived parameters

Test No.	Orifice Diameter (inches)	Inert Particle Diameter (inches)	BP Weight (grams)	Peak Pressure (psia - 5 point average)	Depth of Penetration (inches)	Mass Flow Rate (kg/s)	Froude Number $U_o^2 d_p/(g d_o^2)$	Reynolds Number $\dot{m}/(\mu d_o)$
1	0.065	0.0551	0.1811	2353.48	1.079	1.095E+05	8.352E+13	1.363E+08
2	0.065	0.0551	0.1827	2198.5	1.275	1.023E+05	8.352E+13	1.273E+08
3	0.065	0.0551	0.0858	2238.42	1.220	1.041E+05	8.352E+13	1.297E+08
4	0.065	0.0551	0.0884	1959.8	1.075	9.115E+04	8.352E+13	1.135E+08
5	0.073	0.0551	0.1827	2390.64	0.695	1.402E+05	8.352E+13	1.555E+08
6	0.073	0.0551	0.1849	2724.32	0.696	1.598E+05	8.352E+13	1.772E+08
7	0.073	0.0551	0.0855	2157.58	0.957	1.266E+05	8.352E+13	1.404E+08
8	0.073	0.0551	0.0884	2195.9	0.655	1.288E+05	8.352E+13	1.429E+08
9	0.073	0.0551	0.184	2892.74	1.159	1.697E+05	8.352E+13	1.882E+08
10	0.065	0.0551	0.1842	2538.08	0.969	1.180E+05	8.352E+13	1.470E+08
11	0.065	0.0551	0.0864	2613.4	0.808	1.216E+05	8.352E+13	1.514E+08
12	0.073	0.0551	0.087	2771.14	1.116	1.626E+05	8.352E+13	1.803E+08
13	0.065	0.0669	0.184	2696.18	0.825	1.254E+05	5.665E+13	1.562E+08
14	0.065	0.0669	0.1801	2699.66	0.829	1.256E+05	5.665E+13	1.564E+08
15	0.073	0.0669	0.1822	1634.46	0.807	9.588E+04	5.665E+13	1.063E+08
16	0.073	0.0669	0.1836	2754.16	0.969	1.616E+05	5.665E+13	1.792E+08
17	0.065	0.0669	0.1816	2672.9	0.916	1.243E+05	5.665E+13	1.548E+08
18	0.073	0.0669	0.1835	2104.72	1.070	1.235E+05	5.665E+13	1.369E+08
19	0.0595	0.0551	0.1838	2474.98	0.885	9.646E+04	8.352E+13	1.312E+08
20	0.055	0.0551	0.18	2865.18	1.269	9.541E+04	8.352E+13	1.404E+08
21	0.055	0.0551	0.1828	1989.12	1.115	6.624E+04	8.352E+13	9.749E+07
22	0.055	0.0551	0.1813	2767.36	0.979	9.215E+04	8.352E+13	1.356E+08
23	0.055	0.0669	0.1817	3039.6	0.913	1.012E+05	5.665E+13	1.490E+08
24	0.055	0.0669	0.1834	2912.68	0.732	9.699E+04	5.665E+13	1.428E+08

Figure D1: Summary of condensed phase deposition onto inert bed

44